

Blind Federated Learning via Over-the-Air q-QAM

Saeed Razavikia[†], José Mairton Barros Da Silva Júnior*, Carlo Fischione[†]

[†]School of Electrical Engineering and Computer Science, KTH Royal Institute of Technology, Stockholm, Sweden

*Department of Information Technology, Uppsala University, Uppsala, Sweden

Email: [†]{sraz, carlofi}@kth.se, * mairton.barros@it.uu.se

arXiv:2311.04253v2 [eess.SP] 19 Apr 2024

Abstract—In this work, we investigate federated edge learning over a fading multiple access channel. To alleviate the communication burden between the edge devices and the access point, we introduce a pioneering digital over-the-air computation strategy employing q-ary quadrature amplitude modulation, culminating in a low latency communication scheme. Indeed, we propose a new federated edge learning framework in which edge devices use digital modulation for over-the-air uplink transmission to the edge server while they have no access to the channel state information. Furthermore, we incorporate multiple antennas at the edge server to overcome the fading inherent in wireless communication. We analyze the number of antennas required to mitigate the fading impact effectively. We prove a non-asymptotic upper bound for the mean squared error for the proposed federated learning with digital over-the-air uplink transmissions under both noisy and fading conditions. Leveraging the derived upper bound, we characterize the convergence rate of the learning process of a non-convex loss function in terms of the mean square error of gradients due to the fading channel. Furthermore, we substantiate the theoretical assurances through numerical experiments concerning mean square error and the convergence efficacy of the digital federated edge learning framework. Notably, the results demonstrate that augmenting the number of antennas at the edge server and adopting higher-order modulations improve the model accuracy up to 60%.

Index Terms—blind federated learning, digital modulation, federated edge learning, over-the-air computation

I. INTRODUCTION

In recent years, the surge in mobile device utilization coupled with advancements in sensing and machine learning technologies has facilitated the easy acquisition of mobile data to train machine learning models. Despite this, the heterogeneous and decentralized nature of these data poses a significant challenge. This is particularly evident if one wants to guarantee the optimal performance of models trained locally on individual devices when applied to data from other devices. One potential solution is centralizing data from various devices to a cloud repository for collaborative model training. However, this strategy is often impractical due to substantial communication costs, data privacy issues, and different device hardware specifications [1].

An alternative approach gaining traction is federated learning (FL), wherein a central node aggregates local models from numerous devices to formulate a more refined global model while maintaining data privacy by keeping datasets localized on respective devices. In this scenario, the edge server (ES) oversees the progression of the global model [2], [3]. Devices compute local model updates utilizing their respective data and send them to the ES, aggregating these updates to enhance the

global model. This methodology has been further developed into federated edge learning (FEEL), integrating FL with edge computing to reduce communication overhead by facilitating the transmission of models to an ES for aggregation into a cohesive model [4].

However, this approach has limitations. As the number of devices engaged in FEEL increases, or as the dimensions of local gradients expand, the wireless resources at the network, such as bandwidth and time, may become strained [5]. To mitigate this, over-the-air computation (OAC) has been proposed [6]. This technique concurrently allocates resources to all users, utilizing the waveform superposition of wireless signals. Furthermore, traditionally OAC employs precise analog signal precoding to facilitate the computation of specific functions over-the-air, such as arithmetic means or weighted sums, thereby enhancing efficiency in the use of the resources of the wireless channel [7], [8]. However, most previous studies have focused on analog modulations for OAC and FEEL. Digital modulations would be much more favorable due to their widespread use and error-correction coding capabilities.

Here, we aim to design a new FEEL scheme, where the edge device uses digital modulation instead of the traditional analog modulation for communication via the OAC technique. Adopting digital modulation in OAC and retaining the benefits of the analog approach allows us to move one step towards deploying OAC with current wireless technologies and to address the FEEL challenges, such as communication costs and data privacy, without waiting for the (perhaps economically hard to think) re-introduction of analog communications.

A. Literature Review

Recent developments in the FEEL framework have witnessed the exploration of advanced signal processing techniques, such as beamforming at the ES, equipped with multiple antennas, is underway to augment the quality of the estimated signal utilized in global model updates. Notably, research has been conducted to maximize the number of devices participating in each communication round of training through the implementation of beamforming at the ES [9]. Additionally, innovative nonlinear estimation methods have been developed to precisely recover the sum of updates transmitted by devices, leveraging the inherent sparsity of these updates [10], [11]. Recent studies have also addressed time synchronization errors, with particular emphasis on formulating misaligned OAC into an atomic norm minimization problem to develop synchronization-free estimators [12]–[14]. Moreover, in [11],

[15]–[17], they studied FEEL problem over wireless fading multiple access channel (MAC).

In parallel, the FEEL domain has observed substantial advancements in digital aggregation methods for wireless communication in federated learning applications. The one-bit broadband digital aggregation (OBDA) method, outlined in [18], aims at reducing data communication, thereby conserving bandwidth and energy. Another significant development is adopting majority vote frequency-shift keying (FSK) techniques [17], which aims at harnessing modulation techniques for efficient and reliable data aggregation in wireless networks. Moreover, a phase asynchronous orthogonal frequency division multiplexing (OFDM)-based variant of OBDA has been introduced [19], characterized by the integration of joint channel decoding and aggregation decoders, specifically designed for digital OAC applications, enhancing privacy and efficiency by eliminating the necessity for raw data sharing.

Nevertheless, these OBDA-centric methods exhibit certain limitations, predominantly confined to specific functions such as sign detection and particular machine learning training procedures, such as the signSGD problem [20]. To widen the class of functions for digital OAC, authors in [21] use balanced number systems for computing summation functions. Despite its potential, this approach requires the allocation of unique frequencies for each quantized level, thus raising concerns regarding resource usage and spectral efficiency.

Recently, in [22]–[24], we introduced a fundamentally new communication for computation framework called ChannelComp, which allows for the computing of arbitrary functions over the MAC with digital modulations. ChannelComp offers a spectral efficient communication scheme through digital modulation for the OAC problem, which has several computational benefits compared to analog OAC and OBDA methods and is fully compatible with existing digital communication systems.

B. Our Contribution

In this work, we propose a novel and general digital framework for FEEL, termed ChannelCompFed, which leverages OAC over a wireless fading MAC using q-QAM modulations. The ChannelCompFed methodology is crafted to implement digital OAC, thereby preserving the spectral efficiency intrinsic to digital systems. A significant feature of the ChannelCompFed framework is the elimination of the necessity for edge devices to be aware of the channel state information (CSI), marking a significant deviation from conventional practices in over-the-air computation over a wireless fading MAC, where each transmitting device modulates its transmission based on the instantaneous channel state to ensure signal convergence at the same power level at the ES.

ChannelCompFed strategically integrates multiple antennas at the ES to mitigate the fading phenomena inherent in wireless channels, thus enhancing its operational capabilities. ChannelCompFed builds on the concept proposed in ChannelComp [22], a fully digital OAC method where constellation points at the receiver are sufficiently spaced to allow the function computation. Moreover, ChannelCompFed adopts a digital coding scheme proposed in [24], facilitating computations

over-the-air and promoting ultra-low latency communication while retaining the benefits of digital modulations. Contrary to the uncoded approaches presented in [15], [16], ChannelCompFed utilizes high-order quadrature amplitude modulation (QAM) to amplify the communication rate, thereby enhancing communication reliability and fostering superior gradient estimation, which in turn accelerates convergence during the learning process. We highlight that, unlike the ChannelComp that designs new modulations diagram for computing general functions, ChannelCompFed uses a closed-form coding scheme tailored high order QAM to compute the mean function critical for FEEL.

Furthermore, we establish the theoretical performance of the ChannelCompFed framework. We conduct a meticulous analysis to determine the optimal number of antennas at the ES necessary to counteract the wireless channel’s fading effectively. We theoretically analyze the function computation’s mean squared error (MSE) for noisy and fading scenarios, considering QAM modulations of arbitrary order. To complement our theoretical insights, we prove the convergence of ChannelCompFed, thus providing a theoretical guarantee that verifies its performance efficacy. We illustrate these theoretical propositions through numerical experiments designed to evaluate ChannelCompFed’s proficiency using the MNIST and CIFAR-10 datasets as benchmark.

In summary, our contributions are as follows:

- **Digital federated edge learning:** We consider a digital OAC scheme, termed ChannelCompFed, for the FEEL problems fully compatible with arbitrary order of QAM digital communication systems. The ChannelCompFed method improves the communication rate while proving reliable communication in FEEL network.
- **No CSI information at edge device:** Employing multiple antennas at ES allows us to design a receive beamformer for compensating the effect of fading. Hence, edge devices do not require knowledge of their CSI, and the ES only needs to estimate the sum of the channel coefficients of all the edge devices to each antenna instead of each individual channel coefficient.
- **Required number of antennas:** We provide the analysis for the required number of antennas, N_r , at the ES to obtain an upper bound for the MSE of the gradient over fading MAC. In particular, we obtain a probabilistic lower bound on the number of required antennas at the ES and show that the number of antennas has an inverse relation to the variance of the error, σ^2 , i.e., $N_r = \mathcal{O}(1/\sigma^2)$.
- **MSE analysis and Convergence rate:** We further derive the MSE analysis of the gradient for both noisy and fading MAC conditions, considering QAM modulations of arbitrary order. Utilizing the derived MSE expressions, we establish a convergence analysis for non-convex loss functions, articulating this in terms of the MSE or the estimated gradient over the MAC.
- **Numerical experiments:** We illustrate the theoretical claims and assess the ChannelCompFed framework’s performance effectiveness via numerical experiments. These experiments evaluate the algorithm’s performance over fading channels and utilize the MNIST and the

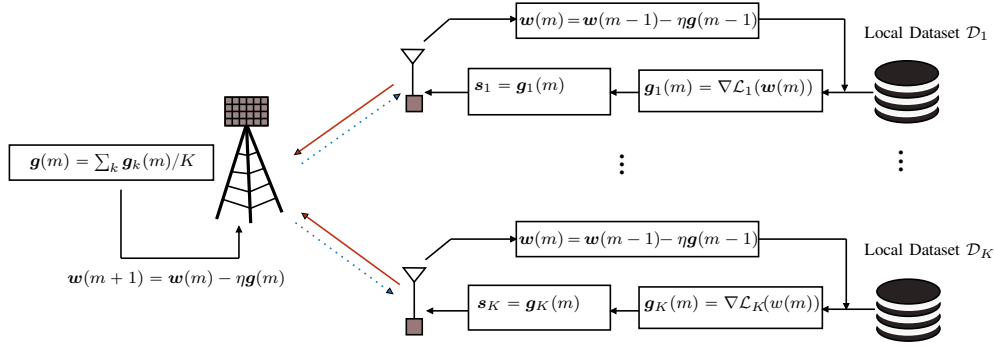


Figure 1. Diagram of federated edge learning where we assume to perform over-the-air computation by the digital modulation QAM. Here, dashed arrow lines (blue color) show the downlink transmission, where the ES sends the updated global model in Eq. (3) back to the edge device. The red lines show the uplink phase, where device k transmits the parameters of the trained model with its local data using modulated signal s_k in Eq. (4) to the server ES.

CIFAR-10 datasets as a benchmark for homogeneous and heterogeneous data distributions. It is observed that increasing the number of receiver antennas and order of modulation by factors 8 and 2, respectively, can lead to approximately 60% of improvements in the model's accuracy for classification problems.

C. Organization of The Paper

The remainder of this paper is organized as follows. Section II presents the learning and communication models for the proposed OAC system. In Section IV, we introduce the ChannelCompFed framework and establish its performance in terms of MSE and convergence rate for the FL problem. Then, we provide the numerical experiments to assess the performance of the proposed scheme in Section V, followed by the concluding remarks in Section VI.

D. Notations

The scalars are represented by lowercase letters, such as x , whereas vectors are denoted by lowercase boldface letters, \mathbf{x} . The transpose of a vector \mathbf{x} is indicated by \mathbf{x}^T , and its Hermitian is represented by \mathbf{x}^H . Given two arbitrary vectors, \mathbf{a} and \mathbf{b} , the notation $\langle \mathbf{a}, \mathbf{b} \rangle$ represents the inner product $\mathbf{b}^H \mathbf{a}$. When referring to a vector \mathbf{x} , $\|\mathbf{x}\|$ denotes its ℓ_2 norm. For a complex scalar x belonging to the set \mathbb{C} , the real and imaginary parts of x are represented by $\Re(x)$ and $\Im(x)$, respectively.

In the context of sets, if S is a set, its cardinality is denoted by $|S|$. For an integer N , the notation $[N]$ is used to represent the set $\{1, 2, \dots, N\}$. The Normal distribution with variance σ^2 is expressed as $\mathcal{N}(0, \sigma^2)$. Additionally, $\mathcal{CN}(0, \sigma^2)$ denotes a circularly symmetric complex Normal distribution, wherein the real and imaginary terms are each distributed according to $\mathcal{N}(0, \sigma^2)$.

II. SYSTEM MODEL

In this section, we provide the learning and communication models used in both the uplink and the downlink.

A. Learning Model

In the FEEL framework [2], [4], [25], our system model operates within a distributed learning scenario involving K edge devices together with an ES to train a shared global model, \mathbf{w} , without sharing their private data. In this regard, each device k holds a distinct local training dataset, labeled as \mathcal{D}_k , where $|\mathcal{D}_k|$ is the number of samples in edge device k . The local loss function used by edge device k is denoted by $\mathcal{L}_k(\mathbf{w})$, where $\mathbf{w} \in \mathbb{R}^N$ represents the model parameters with size N . In the centralized learning approach, the ES utilizes the data across all devices, i.e., $\mathcal{D} := \mathcal{D}_1 \cup \dots \cup \mathcal{D}_K$, and then undertakes the training of the global model by minimizing the empirical loss function in a distributed fashion:

$$\begin{aligned} \mathbf{w}^* &= \underset{\mathbf{w}}{\operatorname{argmin}} \mathcal{L}(\mathbf{w}) = \underset{\mathbf{w}}{\operatorname{argmin}} \frac{1}{|\mathcal{D}|} \sum_k |\mathcal{D}_k| \mathcal{L}_k(\mathbf{w}), \\ &= \underset{\mathbf{w}}{\operatorname{argmin}} \frac{1}{|\mathcal{D}|} \sum_{j \in \mathcal{D}} \ell_j(\mathbf{w}), \end{aligned} \quad (1)$$

where $\mathcal{L}(\mathbf{w})$ denotes the global loss function of the model vector \mathbf{w} , and $\ell_j(\mathbf{w})$ is the empirical loss function calculated for the j -th data sample of the dataset \mathcal{D} .

In a bid to ensure privacy, the FL approach has been proposed. In FL, each device employs its local dataset \mathcal{D}_k for conducting stochastic gradient descent (SGD) for the minimization of the local loss function $\mathcal{L}_k(\mathbf{w})$. Moreover, let $\mathbf{w}_k(m) \in \mathbb{R}^N$ and $\mathbf{g}_k(m) \in \mathbb{R}^N$ denote the local model parameters and gradient estimation of device k at the m -th communication round, respectively. Specifically, in communication round m , device k computes $\mathbf{g}_k(m)$ gradient over its local data set \mathcal{D}_k as

$$\mathbf{g}_k(m) = \frac{1}{|\mathcal{D}_k|} \sum_{j \in \mathcal{D}_k} \nabla \ell_j(\mathbf{w}_k(m)). \quad (2)$$

Next, each device's local model update $\mathbf{g}_k(m)$ is sent to the ES. On receipt of gradient, the ES calculates the global model of the gradient $\mathbf{g}(m)$ across all K devices as:

$$\mathbf{g}(m) = \frac{1}{K} \sum_{k=1}^K \mathbf{g}_k(m). \quad (3)$$

Finally, the ES then updates the current global model by $\mathbf{w}(m+1) = \mathbf{w}(m) - \eta \mathbf{g}(m)$ where η represents the learning rate. Afterward, the updated global model is broadcast back to the edge devices, and the process repeats until a convergence

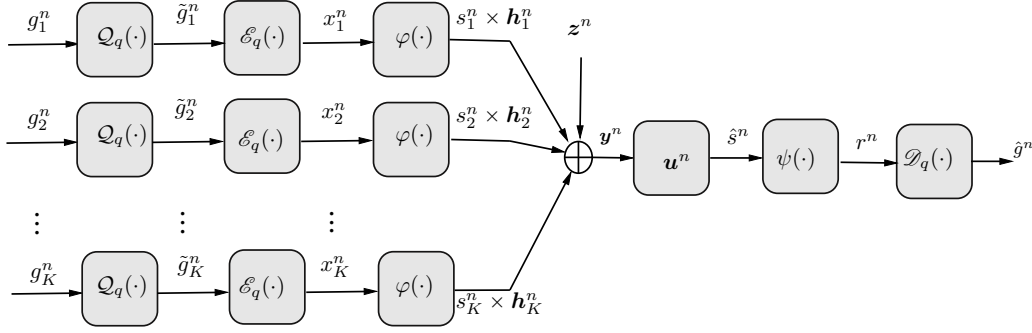


Figure 2. Block diagram illustrating the communication model for FEEL at the n -th communication subchannel. The gradients $g_1^n, g_2^n, \dots, g_K^n$ are first quantized using operator $\mathcal{Q}_q(\cdot)$, and then go through an encoder, $\mathcal{E}_q(\cdot)$, and the pre-processing function, φ . Then, all edge devices transmit the modulated signals $s_1^n, s_2^n, \dots, s_K^n$ over the MAC resulting in the received vector \mathbf{y}^n , which is degraded by the noise \mathbf{z}^n and the wireless channel effects \mathbf{h}^n . The received signal by N_r antennas is \mathbf{y}^n , which undergoes a receiver beamforming vector, \mathbf{u}^n , at the ES. Then, the resultant signal is passed through the post-processing function ψ to obtain n -th element of the received vector \mathbf{r} , i.e., r^n . Finally, r^n is decoded by the decoder $\mathcal{D}_q(\cdot)$ to yield the estimated function \hat{g}^n .

criterion, such as the maximum number of communication rounds or convergence to a local minimum, has been reached. We note that in Eq. (3), the ES requires only the aggregation of local estimates $\mathbf{g}_k(m)$ and not individual gradients from each edge device. Therefore, we can use FEEL, in which the per-round communication latency is independent of the number of ES. This is a benefit of FEEL compared to the traditional multiplexing methods, such as time multiplexing and frequency multiplexing, in which the per-round communication latency and bandwidth increase linearly by the number of ESs, respectively. The overall learning procedure is depicted in Figure 1.

To alleviate the notation, we omit the index m from $\mathbf{g}(m)$ and represent the gradient at each communication round as \mathbf{g} because the communication protocol remains constant across the communication rounds.

B. Communication Model

We assume that the ES is equipped with N_r transmitter/receiver antennas, and every edge device has a single transmitter/receiver antenna. In each communication round, the edge device k needs to transmit its gradient \mathbf{g}_k by the q-QAM modulated signal $x_k \in \mathbb{C}$ to the ES over a broadband MAC. In order to manage frequency-selective fading and intersymbol interference, OFDM is employed, i.e., fractionating the bandwidth B into N orthogonal subchannels¹.

In particular, to perform a digital transmission, the procedure is the following: element n of the gradient vector of edge device k , g_k^n , is quantized into a scalar, $\tilde{g}_k^n := \mathcal{Q}_q(g_k^n)$, with q possible values for $n \in [N]$, where $\mathcal{Q}_q(\cdot)$ is the quantizer and q is the number of quantization levels. Then, the resultant vector is mapped into the digitally modulated signal x_k^n using the encoder $\mathcal{E}_q(\cdot)$, i.e., $x_k^n = \mathcal{E}_q(\tilde{g}_k^n)$. To prevent the transmission power from influencing the learning rate [27], we normalize and denormalize the modulated signals, x_k^n , using

a pre-processing function, φ_k , and post-processing function, ψ , at edge device k and the ES, respectively. Specifically, edge device k first encodes x_k^n into s_k^n using a pre-processing function φ_k as follows:

$$\mathbf{s}_k := \varphi_k(\mathbf{x}_k) = \frac{D_k \mathbf{x}_k}{\sqrt{\beta}}, \quad (4)$$

where β is scaling factor that is chosen to satisfy a transmit power constant for edge devices and $\mathbf{x}_k := [x_{k,1}, \dots, x_{k,N}]^T \in \mathbb{C}^N$ and $\mathbf{s}_k := [s_{k,1}, \dots, s_{k,N}]^T \in \mathbb{C}^N$ and where recall that \mathcal{D}_k is dataset of device k . For a more realistic approach, we consider that the average transmission power of every edge device is limited by a predefined positive value, P_{\max} . With the given transmitted symbols in Eq. (4), we can define the power constraints as follows:

$$\mathbb{E}[\|\mathbf{s}_k\|^2] \leq P_{\max}, \forall k \in [K]. \quad (5)$$

Consequently, we have $\beta \geq \mathbb{E}[\|D_k\|^2 \|\mathbf{x}_k\|^2] / P_{\max}$, which means that $\beta \geq \max_k \{\mathbb{E}[\|D_k\|^2 \|\mathbf{x}_k\|^2]\} / P_{\max}$. Note that higher β reduces the transmitted power, diminishing the SNR and impairing performance. However, the exact values of lower bounds are unavailable in practical scenarios due to the unknown magnitude of gradients beforehand. Consequently, the lower bounds must be approximated and β chosen slightly above the lower bounds to ensure the power constraint in (5) holds.

In the uplink transmission step, all the nodes transmit simultaneously² and over the same subchannel. Afterwards, the ES server receives the summation of all \mathbf{s}_k 's over the MAC during one-time slot [23], i.e.,

$$\mathbf{y}^n = \sum_{k=1}^K \mathbf{h}_k^n s_k^n + \mathbf{z}^n, \quad n \in [N], \quad (6)$$

where \mathbf{y}^n is physically generated by the superposition of electromagnetic waves over-the-air in the wireless channels. Moreover, the n -th element of $\mathbf{h}_k^n \in \mathbb{C}^{N_r}$ denotes the channel coefficient between node k and the ES server at n -th sub-channel and is distributed according to $\mathcal{CN}(\mathbf{0}, \sigma_h^2 \mathbf{I}_{N_r})$;

¹For the ease of explanation, we assume that the number of orthogonal subchannels, B , equals the size of model parameters vector \mathbf{w} , i.e., N . However, extension to an arbitrary number is straightforward, and one can divide the number of model parameters into the number of available communication resources, such as subchannels and time slots, and perform multiple transmissions over different subchannels and time slots [16], [26].

²All nodes and the ES are presumed to achieve perfect synchronization. However, in cases of synchronization imperfections, analog OAC strategies [13], [14], can be implemented.

the term \mathbf{z}^n represents the additive white Gaussian noise (AWGN), which is distributed according to $\mathcal{CN}(\mathbf{0}, \sigma_z^2 \mathbf{I}_{N_r})$. Moreover, different entries of \mathbf{h}_k^n and \mathbf{z}^n can be correlated while the vectors are independent and identically distributed (iid) across ES antennas and subchannels of edge devices.

Next, the ES server applies the receiver beamforming vector $\mathbf{u}^n \in \mathbb{C}^{N_r}$ to the received signal \mathbf{y}^n , and it yields

$$\hat{s}^n := \langle \mathbf{u}^n, \mathbf{y}^n \rangle = \sum_{k=1}^K \langle \mathbf{u}^n, \mathbf{h}_k^n s_k^n \rangle + \langle \mathbf{u}^n, \mathbf{z}^n \rangle. \quad (7)$$

Now, we need to set the beamforming vector \mathbf{u}^n to reduce the influence of the distortion caused by noise \mathbf{z}^n and improve the performance of over-the-air computation. To this end, following the blind transceiver design [15], [16], we set $\mathbf{u}^n = \sum_{k=1}^K \mathbf{h}_k^n / N_r \sigma_h^2$, which yields

$$\hat{s}^n = \sum_{k=1}^K \frac{\|\mathbf{h}_k^n\|^2}{\sigma_h^2 N_r} s_k^n + \sum_{k, k', k \neq k'} \frac{\langle \mathbf{h}_k^n, \mathbf{h}_{k'}^n \rangle}{\sigma_h^2 N_r} s_{k'}^n + \sum_{k=1}^K \frac{\langle \mathbf{h}_k^n, \mathbf{z}^n \rangle}{\sigma_h^2 N_r}. \quad (8)$$

Next, let us consider that \mathbf{h}_k^n and $\mathbf{h}_{k'}^n$ are statistically independent³. Then, for a large number of antennas, $N_r \gg 1$, the signal terms approaches to [28]

$$\|\mathbf{h}_k^n\|^2 / N_r \approx \sigma_h^2, \quad (9a)$$

$$\langle \mathbf{h}_k^n, \mathbf{h}_{k'}^n \rangle / N_r \approx 0, \quad (9b)$$

$$\langle \mathbf{h}_k^n, \mathbf{z}^n \rangle / N_r \approx 0, \quad (9c)$$

where σ_h^2 is the variance of channel coefficients. Then, by substituting Eqs. (9) into Eq. (8), we obtain

$$\hat{s}^n \approx \sum_{k=1}^K s_k^n, \quad n \in [N]. \quad (10)$$

Next, the ES applies the post-processing function of ψ on the received vector $\hat{\mathbf{s}}$ to denormalize it as,

$$\mathbf{r} = \psi(\hat{\mathbf{s}}) = \frac{\sqrt{\beta} \hat{\mathbf{s}}}{\sum_{k=1}^K |\mathcal{D}_k|}. \quad (11)$$

Finally, the ES uses the decoder \mathcal{D} to obtain the global gradient descent direction, i.e., $\hat{\mathbf{g}} = \mathcal{D}(\mathbf{r})$. This communication architecture is summarized in Figure 2. Note that in (10), it is assumed that a large enough N_r can counteract the effects of fading and channel noise. The details and analysis of how many antennas are needed for this approximation are discussed in Section IV.

Remark 1. *The approximation in (10) is a fundamental aspect of our proposed blind transceiver scheme, which aligns with the principles underlying Massive MIMO systems [28] whose feasibility in 5G technologies is promising [29].*

³In case \mathbf{h}_k^n and $\mathbf{h}_{k'}^n$ are correlated, the second term corresponds to an interference error that does not disappear and induces bias error. Let $\sigma_{k, k'}^2$ be the covariance between channels of node k and k' . Regardless of s_k^n , the performance of OAC is degraded proportional to the ratio of $\sigma_{k, k'}^2 / \sigma_k^2$. Suppose the normalized covariance matrix of the nodes channel deviates from the identity matrix. In that case, the error subsequently increases, i.e., $\sigma_{k, k'}^2 \approx \sigma_k^2$ then the expected value of the induces bias \bar{e}_{int}^n increases, where $\bar{e}_{\text{int}}^n := \sum_{k, k', k \neq k'} \sigma_{k, k'}^2 s_k^n / \sigma_h^2$ for $n \in [N]$. To better capture the statistical behavior of the error, we need to analyze the random variables in the interference terms. Regardless of the statistical dependence of \mathbf{h}_k^n and $\mathbf{h}_{k'}^n$, Lemma 3 shows how fast the tails of the random variable in interference deviate from their expected values.

Remark 2. *The ES needs to estimate the receiver beamforming vector \mathbf{u} . However, estimating the accumulative channel gains from all nodes towards each antenna hinders the estimation of individual channel gains \mathbf{h}_k . In other words, this approach reduces the channel estimation overhead, a more noticeable decrease with an increase in the number of devices K or the number of the ES antennas N_r . Indeed, this overhead is invariant concerning K . Moreover, given that \mathbf{h}_k follows a $\mathcal{CN}(\mathbf{0}, \sigma_h^2 \mathbf{I}_{N_r})$ distribution, accordingly, \mathbf{u}^n obtain a Normal distribution as $\mathcal{CN}(\mathbf{0}, \frac{K}{N_r} \mathbf{I}_{N_r})$. Consequently, for sufficiently large N_r , i.e., $N_r \gg 1$, the receiver beamforming vector tends towards an identity vector, facilitating its estimation.*

In the next section, we propose the architecture of the encoder \mathcal{E}_q and decoder \mathcal{D} in detail.

III. CHANNELCOMPFEED: ENCODING AND DECODING

The core concept of ChannelCompFed involves integrating ChannelComp with FEEL to enhance communication efficiency via digital modulation. To this end, we must design the digital encoders and decoders of the system model to provide a low-latency aggregation for the FEEL problem (diagram depicted in Figure 2). This section explains the necessary coding and decoding schemes for its implementation.

A. Encoder and Decoder

This subsection describes how to design the encoder and decoder of ChannelCompFed. For ease of explanation, we consider the scenario where the number of antennas at ES, N_r , is large enough to compensate for the channel effects, and local datasets are assumed to have uniform sizes, i.e., $|\mathcal{D}_k| = |\mathcal{D}|/K$ for $k \in [K]$. With this consideration, Eq. (11) becomes

$$\mathbf{r}^n = \frac{1}{K} \sum_{k=1}^K x_k^n, \quad n \in [N], \quad (12)$$

where ψ and φ_k set to be $1/K$ and identity functions, respectively. Note that x_k^n is a digitally modulated signal, and the superposition of several digitally modulated signals does not necessarily result in valid constellation points. Indeed, the constellation points of digital modulations may overlap, so we cannot assign any function output to the points [23]. For example, using Gray code for the QAM modulation leads to an incomprehensible constellation diagram [24]. To overcome this limitation, we propose to use the non-overlapping coding idea of ChannelComp [22] and the specific coding scheme we proposed in [24].

To illustrate, let us consider a simplified computation scenario involving $K = 2$ nodes, where the objective is to compute the sum function $f(s_1, s_2) = s_1 + s_2$ where $s_1, s_2 \in \{0, 1, 2, 3\}$ using Gray coded PAM with four constellation points. i.e., $x_k = (s_k + \lfloor s_k/2 \rfloor - 2\lfloor s_k/3 \rfloor - 3)E_s/2$ for $k = 1, 2$, where E_s denotes the amplitude of the carrier signal. Then, for the $x_1 + x_2$ the constellation points are given by $r_i = (i - 4) \times E_s$ for $i \in \{1, \dots, 7\}$. In this context, a unique challenge arises: certain constellation points, specifically r_3, r_4 , and r_5 , may be required to simultaneously represent multiple sum values ($\{3, 2, 3\}$ and $\{2, 4, 6\}$). This

overlap creates ambiguity, as exemplified when nodes 1 and 2 transmit values of $s_1 = 1$ and $s_2 = 1$, resulting in the constellation point r_3 , and similarly, $s_1 = 0$ and $s_2 = 3$ also mapping to r_3 . Such conflicts prevent accurate computation of the desired sum at the ES, showcasing the inherent limitation of traditional coding schemes in digital OAC.

To encode every value of gradient g_k^n of node k , we use QAM of order q , which represents the quantization level. Without loss of generality, we let the quantized elements of the gradient be integers, i.e., $\tilde{g}_k^n \in [0, \dots, q-1]$ for all $n \in [N]$ and $k \in [K]$. Then, we propose the encoder $\mathcal{E}_q(\cdot) : \mathbb{Z} \mapsto \mathbb{C}$ for scalar $g \in \mathbb{Z}$ as follows

$$[\mathcal{E}_q(g)]_1 := g - 2^b \cdot \lfloor g2^{-b} \rfloor + \frac{1 - 2^b}{2}, \quad (13)$$

$$[\mathcal{E}_q(g)]_2 = \left\lfloor g2^{-b} \right\rfloor + \frac{1 - 2^b}{2}, \quad (14)$$

where $b = 0.5 \log_2(q)$ and $[\mathcal{E}_q(g)]_1$ is equivalent to the modulo operation, and $[\mathcal{E}_q(g)]_2$ is the same as the floor division operation. Then, node k transmits $x_k^n = [\mathcal{E}_q(g)]_1 + j[\mathcal{E}_q(g)]_2 \in \mathbb{C}$ for $n \in [N]$ over the MAC. Conversely, at the receiver, to decode the average global stochastic gradient, i.e., g , we propose the decoder $\mathcal{D}_q : \mathbb{C} \mapsto \mathbb{Z}$ as

$$\begin{aligned} \mathcal{D}_q(x) := & \mathcal{R}(\Re(x)) + 2^b \cdot \left(\mathcal{R}(\Im(x)) + \frac{2^b - 1}{2} \right) \\ & + \frac{2^b - 1}{2}, \end{aligned} \quad (15)$$

where $x \in \mathbb{C}$ and $\mathcal{R}(\cdot)$ is the round up to half function, i.e.,

$$\mathcal{R}(z) = \lceil z + 0.5 \rceil - 0.5. \quad (16)$$

Note that this decoding function works assuming that g is an integer; otherwise, the output becomes the quantized version of input g , i.e., $\tilde{g} \in \{0, \dots, q-1\}$. The decoding and encoding functions \mathcal{D}_q and \mathcal{E}_q satisfy the following property.

Proposition 1. *Let $\tilde{g}_k \in \{0, 1, \dots, q-1\}$ be an integer value for $k \in [K]$ and $\tilde{g} = \sum_{k=1}^K \tilde{g}_k / K \in \{0, 1/K, \dots, q-1 - 1/K, q-1\}$ be the average value. Then, the decoding and encoding functions \mathcal{D}_q and \mathcal{E}_q are identity operators with respect to \tilde{g} , i.e.,*

$$\tilde{g} = \mathcal{D}_q\left(\mathcal{E}_q(\tilde{g})\right) = \frac{1}{K} \mathcal{D}_q\left(\sum_{k=1}^K \mathcal{E}_q(\tilde{g}_k)\right). \quad (17)$$

Proof. See Appendix A. \square

By applying Proposition 1 on each element of the gradient vector \mathbf{g} , we obtain the quantized version of the global model $\tilde{\mathbf{g}} := \sum_{k=1}^K \tilde{\mathbf{g}}_k / K$ as follows:

$$\hat{\mathbf{g}} = \frac{1}{K} \mathcal{D}_q\left(\sum_{k=1}^K \mathcal{E}_q(\mathbf{g}_k)\right) = \tilde{\mathbf{g}}. \quad (18)$$

Therefore, we can successfully compute the average over the MAC with the aforementioned coding scheme.

Remark 3. *The encoding and decoding framework, characterized by equations (13) to (15), offer several advantages over existing schemes. It ensures a unique and non-overlapping representation of aggregated signals, which is critical for accurate OAC computation. The scheme is robust to signal distortion and noise, enhancing the reliability of*

gradient aggregation. It facilitates efficient utilization of the communication channel, optimizing the bandwidth and energy consumption, i.e., there is no need to use orthogonal communication resources to avoid destructive overlaps.

Remark 4. *Note that due to the quantization of the parameter model at edge device k , \mathbf{g}_k , the global model \mathbf{g} becomes also quantized with a finer grid $q' = q \times K$. In the case of a massive number of devices $K \gg 1$, the effect of quantization with q' is negligible compared to the local model grid q . This phenomenon is also reflected in Proposition 2, which shows that the quantization error decreases by a factor of $1/K$. As a result, quantized SGD performs similarly to the vanilla SGD algorithm.*

The proposed coding scheme promotes high-rate communication via over-the-air computation employing high-order QAM modulation, achieving a more effective constellation diagram than its analog equivalent. Note that the computational complexity of ChannelCompFed is almost identical to the analog scheme. Indeed, ChannelCompFed uses the SumComp coding scheme for the communication scheme, whose complexity is analytically studied as detailed in [24]. In the next subsection, the performance of ChannelCompFed with the proposed coding scheme is analyzed.

IV. THEORETICAL CONVERGENCE ANALYSIS

Here, we present the convergence analysis of FEEL problem using the ChannelCompFed framework for both the noisy and fading MAC. We divide this section into two parts; first, we analyze the MSE error on the gradient over the noisy MAC in the following subsection. Then, we provide a probabilistic upper bound on the gradient estimation error in the presence of fading as a function of the number of required antennas.

A. MSE Analysis

To provide the convergence rate of the proposed ChannelCompFed scheme, we need an upper bound on the MSE of induced errors over the MAC. In Proposition 2, we propose an upper bound for describing the MSE error in the AWGN channel where the beamforming vectors have fully compensated the fading effect. In particular, the received signal at ES server is only contaminated by the channel noise, i.e.,

$$\hat{s}^n = \sum_{k=1}^K s_k^n + \tilde{z}^n, \quad n \in [N], \quad (19)$$

where the variance of the noise \tilde{z}^n is reduced by the number of antenna, i.e., σ_z^2 / N_r . In (19), we remove the fading effect as reflected in (6).

Proposition 2. *Consider a communication network with K nodes where each device uses the encoder \mathcal{E} to compute the averaging $\mathbf{g} = \sum_k \mathbf{g}_k / K$, where \mathbf{g}_k is the local gradient of the k -th edge device over the noisy MAC with $\mathcal{CN}(\mathbf{0}, \sigma_z^2 \mathbf{I}_{N_r})$. Assume gradient values are generated uniformly at random with maximum absolute value Δ_g , i.e., $g_k^n \sim \mathcal{U}(-\Delta_g, \Delta_g)$ for $n \in [N]$. Then, the MSE of the computation errors using*

QAM modulation of order of $q = 2^{2b}$ (perfect square number), where $2b$ is the number of bits, is given by

$$\mathbb{E}[\|\mathbf{g} - \hat{\mathbf{g}}\|^2] \leq \sigma_{\text{AWGN}}^2 + \sigma_q^2, \quad (20)$$

where

$$\sigma_{\text{AWGN}}^2 := \frac{N}{K^2}(1+q)e_r, \quad (21)$$

$$\sigma_q^2 := \frac{N\Delta_g^2}{3Kq^2}, \quad (22)$$

in which $\hat{\mathbf{g}}$ is the estimated global gradient received in Eq. (18), and e_r is defined as

$$e_r = 2 \sum_{\ell=1}^{2^b-1} \left(2\ell - 1 \frac{3\ell - 3\ell^2 - 1}{2^b}\right) Q\left(\frac{(2\ell - 1)\sqrt{N_r}}{2\sigma_z}\right), \quad (23)$$

and $Q(\cdot)$ denotes the Q -function.

Proof. The proof is provided in Appendix B. \square

Proposition 2 shows that increasing the modulation order while improving the variance of the quantization σ_q^2 can add noise term to e_r . Also, increasing the number of antennas N_r reduces the error by dampening the variance of the noise.

B. Number of Antennas for Convergence

We recall that in Section II-B, the received signal at the ES experiences fading while the ES can cancel the effects of fading using a large number of antenna N_r . From the law of large numbers, we know that when $N_r \rightarrow \infty$, the interference and the noise terms in Eq. (9) asymptotically vanishes. Consequently, the estimated value of the gradient $\hat{\mathbf{g}}$ approaches the actual value, i.e., \mathbf{g} . Therefore, we here provide a probabilistic lower bound for the number of antennas N_r in the $\hat{\mathbf{g}}$ estimation error. In particular, we prove in Theorem 1 that for large values of N_r and with high probability, the estimation error of $\hat{\mathbf{g}}$ is bounded.

Theorem 1. Consider a communication network with K edge devices and an ES as the server equipped with N_r antennas. Let the complex signal $s_k^n \in \mathbb{C}^N$ be the transmitted signal by the edge device k over the fading channel with coefficients \mathbf{h}_k^n , and let \mathbf{y}^n be the received signal at ES for the n -th sub-channel. Then, the absolute difference between s^n and its estimated value, \hat{s}^n , as well as the expected value of the difference, are bounded, i.e.,

$$|\hat{s}^n - s^n| \leq \epsilon, \quad (24)$$

$$\mathbb{E}[|\hat{s}^n - s^n|] \leq \frac{4K\gamma_n}{\sqrt{N_r c_n}}(\sqrt{\pi} + \ln(6K)), \quad (25)$$

where $c_n = 1/\gamma_n + \sigma_h/\sigma_z$ and γ_n is a positive constant, and N_r fulfills the following lower bound:

$$N_r \geq \frac{8\gamma_n^2 K^2}{\epsilon^2 c_n^2} \ln\left(\frac{6K}{\delta}\right), \quad (26)$$

with probability no less than $1 - \delta$.

Proof. The proof is provided in Appendix C. \square

Proposition 3. Let $\mathbf{g} \in \mathbb{C}^N$ be the global gradient averaged by the ES, and $\hat{\mathbf{g}}$ be the estimated gradient of $\mathbf{g} := \sum_k \mathbf{g}_k/K$, where $\mathbf{g}_k^n \sim \mathcal{U}(-\Delta_g, \Delta_g)$ for $n \in [N]$. Then, with probability no less than $1 - \delta$, the error of the estimated gradient, $\hat{\mathbf{g}}$, as well as the MSE of $\hat{\mathbf{g}}$, are bounded by scalar σ_{fad}^2 , i.e.,

$$\|\tilde{\mathbf{g}} - \hat{\mathbf{g}}\| \leq \epsilon_{\text{fad}}, \quad (27)$$

$$\mathbb{E}[\|\mathbf{g} - \hat{\mathbf{g}}\|^2] \leq \sigma_{\text{fad}}^2 + \sigma_q^2, \quad (28)$$

where

$$\sigma_{\text{fad}}^2 := 16 \frac{N\gamma_{\text{max}}^2 q}{N_r c_{\text{min}}^2} (\pi + 2 \ln(6K))^2, \quad (29)$$

if the number of antennas, N_r , is greater than

$$N_r \geq \frac{16\gamma_{\text{max}}^2 N q}{\epsilon_{\text{fad}}^2 c_{\text{min}}^2} \ln\left(\frac{6K}{\delta}\right), \quad (30)$$

where $\gamma_{\text{max}} := \max_n \gamma_n$, $c_{\text{min}} := \min_n c_n$, and q is the order of modulations.

Proof. The proof is provided in Appendix G. \square

As reflected in Proposition 3, the number of antennas N_r , has an inverse relation with respect to the variance of error, σ_{fad}^2 . Contrary to σ_{AWGN}^2 , σ_{fad}^2 does not improve with the number of edge devices in the network. This is due to the choice of \mathbf{u}^n as the sum of random channel coefficients of K edge devices. Due to the variance of channel coefficients, σ_h^2 , the added randomness makes it challenging to concentrate on the mean because we are averaging over the number of antennas, not the number of edge devices.

C. Convergence Analysis

In this subsection, we prove the convergence analysis of the ChannelCompFed in terms of the optimality gap for the noisy and fading channels. First, we need to present our assumptions on the loss function and the gradients, which are standard in the literature [18], [20], [21].

Assumption 1. (Unbiased average local stochastic gradients) The average stochastic gradient vector $\sum_k \hat{\mathbf{g}}_k(m)/K$ is an unbiased estimate of the global gradient vector $\mathbf{g}(m)$, i.e., $\mathbb{E}[\sum_k \hat{\mathbf{g}}_k(m)/K] = \mathbf{g}(m)$.

Assumption 2. (Smoothness) The gradient of the loss function $\mathcal{L}(\mathbf{w})$ is differentiable and Lipschitz continuous with a non-negative constant L on \mathbb{R}^+ . This means that for any two vectors \mathbf{w} and \mathbf{v} , the following inequalities are satisfied and equivalent:

$$|\mathcal{L}(\mathbf{w}) - \mathcal{L}(\mathbf{v}) - \langle \nabla \mathcal{L}(\mathbf{w}), \mathbf{w} - \mathbf{v} \rangle| \leq \frac{L}{2} \|\mathbf{w} - \mathbf{v}\|, \quad (31)$$

$$\|\nabla \mathcal{L}(\mathbf{w}) - \nabla \mathcal{L}(\mathbf{v})\| \leq L \|\mathbf{w} - \mathbf{v}\|. \quad (32)$$

Assumption 3. (Gradient Divergence) The local gradient estimate \mathbf{g}_k at edge device k is an unbiased estimate of the global gradients \mathbf{g} with bounded variance as

$$\mathbb{E}[\|\mathbf{g}_k - \mathbf{g}\|^2] \leq \theta_k, \quad k \in [K]. \quad (33)$$

Assumption 4. (Unbiased quantization) Let us denote the aggregated gradient with OAC as $\tilde{\mathbf{g}} = \mathbf{g} + \mathbf{e}_q$, where \mathbf{e}_q is

the error due to the quantization. Then, the following upper bound on e_q is satisfied:

$$\mathbb{E}[e_q] = \mathbf{0}_q, \quad \sigma_q^2 := N \frac{\Delta_g^2}{q^2 K} \geq \mathbb{E}[\|e_q\|^2], \quad (34)$$

where Δ_g denotes the maximum value for a gradient element across the whole training procedure, i.e., $\Delta_g := \max_{k,n,m} |g_k^n(m)|$.

Finally, using Assumptions 1-4 and the obtained upper bound on the estimated gradient from Theorem 1 and Proposition 2, we can prove the convergence of the ChannelCompFed scheme for the class of non-convex cost functions as follows.

Proposition 4. Consider a learning rate η . Moreover, consider that Assumptions 1-4, Theorem 1, and Proposition 2 hold. Then, the proposed distributed training scheme, termed ChannelCompFed, converges to a stationary point after performing T communication rounds, with the following convergence rate

$$\begin{aligned} \mathbb{E}\left[\frac{1}{T} \sum_{m=1}^T \|\mathbf{g}(m)\|^2\right] &\leq \frac{1}{T\eta(1 - \frac{\eta L}{2})} \left(\mathcal{L}(\mathbf{w}(1)) - \mathcal{L}^*\right) \\ &+ \frac{\frac{\eta L}{2}}{1 - \frac{\eta L}{2}} \left((\sigma_{\text{ch}}^2 + \sigma_q^2) + \bar{\theta}\right), \end{aligned} \quad (35)$$

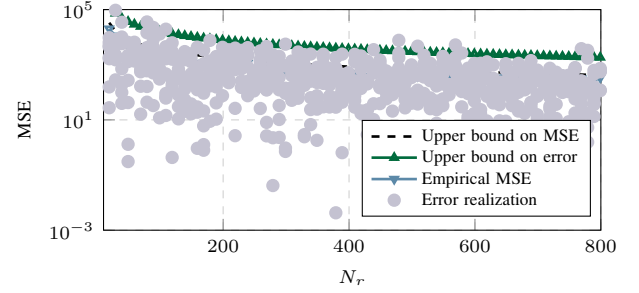
where $\bar{\theta} = \sum_{k=1}^K \theta_k / K$ with θ_k defined in Eq. (33) and $\sigma_{\text{ch}}^2 := \mathbb{E}[\|\mathbf{g}(m) - \hat{\mathbf{g}}(m)\|^2]$.

Proof. The proof is provided in Appendix H. \square

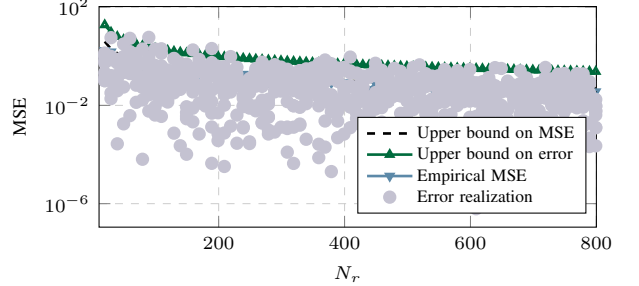
Remark 5. Note that σ_{ch}^2 is the error of gradient estimation caused by the non-idealities of the communication channel. For the case of the noisy and fading MAC, σ_{ch}^2 can be upper bounded by σ_{AWGN}^2 from Eq. (21) and σ_{fad}^2 from Eq. (29), respectively.

Remark 6. In practical wireless systems, electromagnetic interference follows heavy-tailed distributions [30] and [31]. The symmetric α -stable distribution can encapsulate the statistical behavior of such interference. The effect of such distribution in distributed learning through OAC has been studied in [32]. Indeed, it can be shown that the convergence trajectory is reduced by the order of $\mathcal{O}(1/T^{\alpha-1})$, where the parameter α is the tail index. An inversely proportional relationship exists between α and the heaviness of the interference distribution's tail, with a small α resulting in a slow convergence rate for the learning algorithm. However, it is noteworthy that despite the corruption of the aggregated gradient by random channel fading and heavy-tailed interference with potentially infinite variance, gradient descent model training employing a decreasing learning rate can converge to the global optimum regardless of the loss function or the algorithm [32].

In the next section, we evaluate ChannelCompFed with respect to the impact of the error on the MSE for different numbers of antennas and evaluate the learning performance of the ChannelCompFed scheme for distributed learning.



(a) Estimation of s^n



(b) Estimation of \mathbf{g}

Figure 3. Monte Carlo numerical evaluation of the summation function, for 10 trials versus the analytical results from Theorem 1 for $\delta = 0.01$ over different numbers of antennas, N_r . The channel coefficients and channel noise generated by $N(\mathbf{0}, \sigma_h \mathbf{I}_{N_r})$ and $\mathcal{CN}(\mathbf{0}, \sigma_z \mathbf{I}_{N_r})$, respectively, are $\sigma_h = \sigma_z = 1$. Figure 3(a) shows the empirical MSE of \hat{s}^n , analytical upper bound on the error in (24), and expected value in (25) from Theorem 1, for $K = 200$ edge devices. Figure 3(b) shows the empirical and analytical upper bound on the MSE of gradient $\hat{\mathbf{g}}$ from Proposition 3, for $K = 20$ edge devices whose elements of their gradients, \mathbf{g}_k , generated uniformly at random from $\mathcal{U}[-2, 2]$.

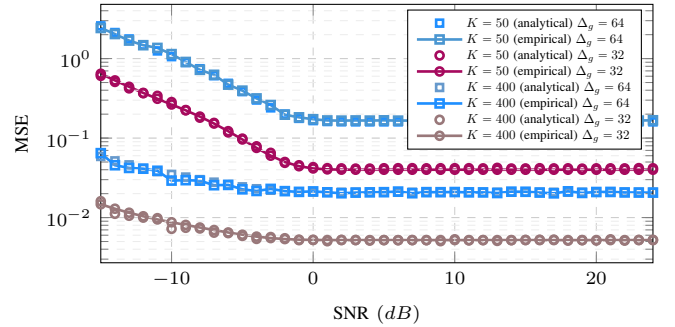


Figure 4. Monte Carlo numerical evaluation of the average gradient estimation in (20) with true gradient, for 100 trials versus the analytical results from Proposition 2. Here, we consider $q = 64$ and $N = 100$ for two cases of $K = 50$ and $K = 400$ edge devices. The gradients \mathbf{g}_k generated uniformly at random from $\mathcal{U}[0, 64]$ and $\mathcal{U}[0, 32]$.

V. NUMERICAL EXPERIMENTS

In this section, we initially conduct a numerical examination of the MSE analysis. Subsequently, we assess the efficiency of the digital ChannelCompFed in terms of learning accuracy and latency over the number of antennas and various modulation orders for homogeneous and heterogeneous data distribution.

A. MSE Analysis

First, we analyze the performance of ES in removing the fading effects for estimating the summation value $s^n =$

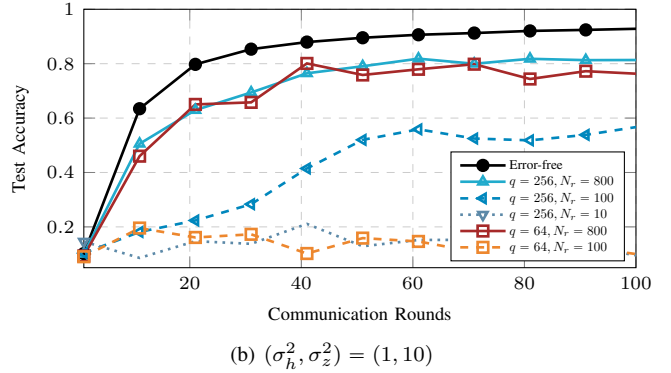
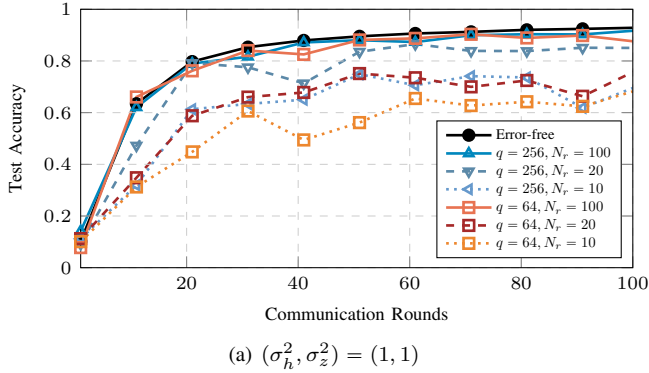


Figure 5. Accuracy of the MNIST task as a function of the communication rounds for $K = 20$ edge devices and heterogeneous data distribution across edge devices. Figures 5(a) and 5(b) show the accuracy of FEEL versus number of communication rounds for two low variance of the noise, i.e., $\sigma_z^2 = 1$ and the high variance of the noise, i.e., $\sigma_z^2 = 10$, respectively.

$\sum_{k=1}^K s_k^n$ in Eq. (10), which results in the estimation of gradient \hat{g} over the fading MAC with $K = 200$ nodes. The transmitted signal by device k , s_k^n , is generated uniformly at random between 0 and 1, i.e., $s_k^n \sim \mathcal{U}[0, 1]$ for $k \in [K]$ and any sub-channel $n \in [N]$. Then, the channel coefficient is generated randomly with Normal distribution, i.e., $h_k \sim \mathcal{CN}(\mathbf{0}, \sigma_h^2 \mathbf{I}_{N_r})$ with $\sigma_h^2 = 1$ for $k \in [K]$, aligning with standard assumptions in the literature, such as [16]. We also generate the channel's noise with the same distribution, i.e., $\mathcal{CN}(\mathbf{0}, \mathbf{I}_{N_r})$. We repeat the experiment over 100 Monte Carlo trials.

In Figure 3, we show the estimation performance of Eq. (10) in terms of the MSE error for different number of antennas at the ES. We also depict both the proposed probabilistic upper bound on the value of the error $|\hat{s}^n - s^n|$ and MSE, from Theorem 1, for comparison with the outage of empirical error values. Furthermore, we show the MSE of estimating the global gradient over the noisy MAC using ChannelCompFed encoder and decoders in (18) and analytical results from Proposition 2 for different numbers of antennas, N_r . Note that the experiments are done for 100 Monte Carlo trials while only 10 trials are depicted in Figure 3.

Figure 3(a) shows the empirical MSE, the analytical upper bound of MSE, and the analytical upper bound on the absolute error $|\hat{s}^n - s^n|$ with the down-side triangle marker, dashed line, and up-side triangle marker, respectively. Also, the circles in Figure 3(a) represent the absolute value of the estimation error from a single realization of the instantaneous Monte Carlo trial.

Similarly, we show the empirical MSE, the analytical upper bound of MSE, and the error for the estimated global gradient \hat{g} with $N = 100$ and $K = 20$ in Figure 3(b). We note that the upper bound on the MSE is well approximated to the true value, which means it predicts the outage of the empirical error well. Moreover, by increasing the number of antennas N_r , the MSE decreases, which is expected due to Theorem 1. This observation is consistent with the theoretical approximation of the MSE in Proposition 3.

Finally, we compute the average performance under the quantization gradient and performance under the true gradient in (20). To this end, we generated edge device gradients g_k

uniformly at random from $\mathcal{U}[0, 32]$ for two cases of $K = 50$ and $K = 400$ edge devices. Then, the gradient's continuous values are quantized by $q = 64$ levels and transmitted by QAM 64 over the noisy MAC in (19). Also, the number of parameters is set to be $N = 100$. This experiment is repeated by changing the distribution of gradients to $\mathcal{U}[0, 64]$ to see the effects of Δ_g on the quantization error.

Figure 4 shows Monte Carlo numerical evaluation of the average gradient estimation in (20) with true gradient for 100 trials versus the analytical results from Proposition 2. As noted by Remark 4, by increasing the number of edge devices K , the quantization error decreases, and ChannelCompFed performs almost equally to vanilla SGD. Moreover, the computation error is positively related to the maximum value for a gradient element, and increasing the maximum value of the gradient results in a higher error. This observation is consistent with the theoretical approximation of the MSE in Proposition 2.

B. Federated Edge Learning

We assess the performance of the proposed digital blind FEEL scheme, i.e., edge devices have no access to the CSI, in terms of the learning of accuracy with respect to the test dataset. We analyze two scenarios: first, including the impact of the number of antennas on the convergence in both homogeneous and heterogeneous data distributions for the FEEL; second, to show the level of improvement for various orders of digital modulations. The machine learning task is image classification for the MNIST [33] dataset and CIFAR-10 [34]. We use the ADAM optimizer [35] to train convolutional neural network (CNN), and the size of the local mini-batch is set to be 128. In the training process, edge devices run 3 epochs per communication round for $T = 100$ global communication rounds.

The FEEL network structure follows the communication model presented in Section II-B with $K = 20$ edge devices. The channel coefficients and noise for all sub-channels are generated according to $h_k^n \sim \mathcal{CN}(\mathbf{0}, \sigma_h^2 \mathbf{I}_N)$ and $z^n \sim \mathcal{CN}(\mathbf{0}, \sigma_z^2 \mathbf{I}_N)$.

For the homogeneous data distribution, the training dataset randomly distributes into K disjoint local datasets, each assigned to an edge device. The local datasets consist of samples

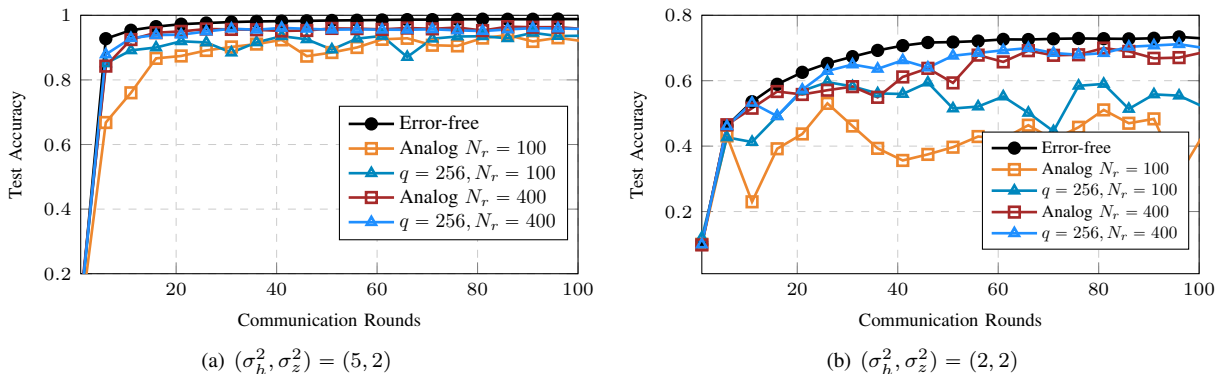


Figure 6. Performance comparison for homogeneous dataset distribution among the edge devices. The accuracy is depicted versus the communication rounds for the error-free baseline, digital FEEL, and the analog FEEL method proposed in [16]. The channel coefficients are generated randomly with variance $\sigma_h^2 = 5$ and $\sigma_z^2 = 2$, for Figure 6(a) and 6(b). Also, the noise follows a Normal distribution with variance $\sigma_z^2 = 2$ and $\sigma_z^2 = 2$ for Figure 6(a) and 6(b), respectively.

with the same labels assigned to each edge device to model heterogeneous data distributions.

The architecture is designed for image classification tasks and comprises two 2D convolutional layers with 20 and 40 filters, both utilizing a 7×7 kernel and ReLU activation. These are followed by 2×2 max-pooling layers. Subsequently, we have a fully connected layer with 2560 units and ReLU activation. A dropout layer with a rate of 0.2 is included for regularization. The output layer is fully connected with 10 units and employs a softmax activation function. The model employs Sparse Categorical Cross-Entropy as the loss function. The total number of parameters is $N = 5,086,010$. Note that this architecture is used for both datasets, and the only difference is the size of the input layer, which is 28×28 for the MNIST and 32×32 for the CIFAR-10 datasets, respectively.

The performance of the proposed digital scheme is compared to the baseline (error-free) and blind FEEL scheme proposed in [16]. In the error-free scheme, there is no noise or fading; therefore, the ES receives perfect copies of the model updates. Moreover, the analog FEEL scheme follows similar communication in Eq. (8) while using analog amplitude modulation instead of the SumComp in our scheme.

In Figure 5, we analyze the impact of the number of antennas on the performance of the ChanneCompFed for different orders of QAM and various levels of noise and fading. Figure 5(a) shows the test accuracy over the communication rounds for various numbers of antennas at the ES, $N_r = \{10, 20, 100\}$, and QAM orders, $q = \{64, 256\}$. Note that increasing the number of antennas makes the convergence faster and helps the final models to reach higher accuracy, as expected according to Proposition 4. Furthermore, increasing the order of modulations from 64 to 256 improves the learning performance, resulting in higher model accuracy after the total communication rounds. Figure 5(b) shows a similar curve for high noise scenarios, now with $\sigma_z^2 = 10$ and number of antennas selected from $N_r = \{10, 100, 800\}$. Due to the high variance of the channel noise, the ES needs to employ both more number of antennas and a higher order of modulation to reduce the effect of fading and noise. This behavior is

noticeable because the ES fails to obtain a good accuracy (at least 60%) for $N_r = 10$ or $q = 64$. In this case, to compensate for the effects of fading and high noise variance, we require employing more antennas ($N_r \geq 800$) and QAM with $q \geq 256$.

The experiments reveal two distinct findings. In the first scenario, for noise scenario with variance on the level of the fading channels, ChanneCompFed works well provided that ES employs either a high number of antennas, N_r , or high order modulation q . However, for a high noise scenario, with 10 times the variance of the fading channel, there is a necessity for high-order modulations coupled with a substantial number of antennas. This event is correctly captured by Theorem 1 and Proposition 3 in terms of scalar c_n .

For the next experiment presented in Figure 6, we use the same learning procedure from Figure 5 but now for homogeneous dataset scenarios for MNIST and CIFAR-10. We compare the performance of ChanneCompFed with $q = 256$ to the analog scheme [16]. We make this comparison to test the accuracy of FEEL over a network with the same number of devices as in Figure 5, but with different numbers of antennas, $N_r = \{100, 400\}$ at the ES. Figure 6(a) shows that the ChanneCompFed and analog FEEL perform well for the homogeneous with $N_r = 400$ antennas for both datasets. However, their performance degrades for the case $N_r = 100$ due to the high fading and noise variances. By increasing the number of antennas N_r for the ES, the performance of both analog and ChanneCompFed asymptotically reaches the error-free baseline. Figure 6(b) shows a similar scenario for $K = 10$ edge devices with different channel noise and fading variances where $\sigma_h^2 = \sigma_z^2 = 2$ for the CIFAR-10 dataset. While both the ChanneCompFed and analog FEEL perform similarly for $N_r = 400$ and $N_r = 100$, ChanneCompFed shows higher accuracy for both cases.

Figure 7 illustrates the communication latency of ChanneCompFed in comparison to analog and orthogonal communication methods for broadband communication with a bandwidth of $B = 1$ kHz. The division of the number of model parameters N by B results in communication rounds taking place across $\lceil N/B \rceil$ time slots. We employ the orthogonal

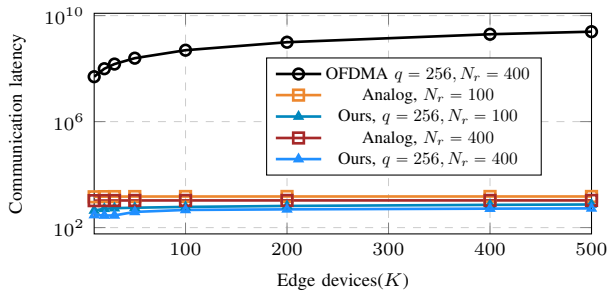


Figure 7. Comparison of latency reduction in FEEL: This figure illustrates the latency reduction achieved by ChannelComFed, analog FEEL, and OFDMA in federated learning tasks, considering a broadband communication setting characterized by a bandwidth of $B = 1$ kHz.

frequency division multiple access (OFDMA) technique for the orthogonal communication, allocating a sub-channel to each edge device for model parameter transmission. As expected, both the analog scheme and ChannelCompFed achieve significantly (10^5 times) lower latency than the conventional orthogonal OFDMA approach. Note that latency is computed based on the rate-distortion function for a fading channel in [36], and the detailed analysis is provided in Appendix I.

We observe that our proposed ChannelCompFed scheme enables existing modulation to train the model over the MAC with similar learning performance for different numbers of antennas while it keeps the benefit of the analog scheme, such as spectral efficiency and low latency communication.

VI. CONCLUSION

In this study, we investigated FEEL over a fading MAC. To alleviate the communication burden, we considered a novel digital OAC scheme, termed ChannelComp, utilizing QAM modulations. This method enables an ultra-low latency communication strategy for addressing the FEEL problem.

Our approach employs multiple antennas at the ES to counteract the detrimental impacts of fading effects inherent in wireless channels. Our theoretical analysis rigorously determined the number of antennas needed at the ES to mitigate the fading effects effectively, shedding light on systems design considerations.

We extended our study to derive our proposed scheme's MSE under noisy and fading MAC conditions. Capitalizing on the obtained MSE expressions, we proved the convergence rate for a non-convex loss function, offering insights into the algorithm's behavior under noisy and fading scenarios.

Our numerical results corroborate the theoretical conclusions concerning MSE and the convergence properties of the digital FEEL framework. These results showed that an enhanced estimation of average local model updates is achievable by augmenting the antenna number at the ES and employing higher-order QAM, improving the model accuracy up to 60%.

In conclusion, this work introduces a viable approach to implementing FEEL over fading MAC and provides rigorous analytical insights and empirical evidence to support its potential as a robust and efficient solution for distributed machine learning in wireless edge computing environments.

APPENDIX

A. Proof of Proposition 1

We first obtain the complex value of $\hat{g} := \sum_{k=1}^K \mathcal{E}_q(\tilde{g}_k)/K$. Then, we apply the decoder function \mathcal{D}_q to the resultant value. In particular, for the real part of the average of encoded gradients, we have

$$\begin{aligned} \mathcal{R}(\Re(\hat{r})) &= \frac{1}{K} \mathcal{R} \left(\sum_{k=1}^K [\mathcal{E}_q(\tilde{g}_k)]_1 \right), \\ &= \frac{1}{K} \mathcal{R} \left(\sum_{k=1}^K \tilde{g}_k - 2^b \sum_{k=1}^K \left\lfloor \frac{\tilde{g}_k}{2^b} \right\rfloor \right) + \frac{2^b - 1}{2}, \\ &= \mathcal{R}(\tilde{g}) + \frac{2^b - 1}{2} - \frac{2^b}{K} \sum_{k=1}^K \left\lfloor \frac{\tilde{g}_k}{2^b} \right\rfloor. \end{aligned} \quad (36)$$

For the imaginary part of \hat{r} ,

$$\mathcal{I}(\Im(\hat{r})) = \frac{1}{K} \mathcal{R} \left(\sum_{k=1}^K [\mathcal{E}_q(\tilde{g}_k)]_2 \right) = \frac{1}{K} \sum_{k=1}^K [\tilde{g}_k 2^{-b}] + \frac{2^b - 1}{2}. \quad (37)$$

Then, by substituting Eqs. (36) and (37) into Eq. (15), we have

$$\frac{1}{K} \mathcal{D}_q \left(\sum_{k=1}^K \mathcal{E}_q(\tilde{g}_k) \right) = \tilde{g}, \quad (38)$$

This concludes the proof.

B. Proof of Proposition 2

Recall that g^n , \tilde{g}^n and \hat{g}^n are the n -th element of gradient \mathbf{g} , quantized gradient $\tilde{\mathbf{g}}$, and the estimated gradient $\hat{\mathbf{g}}$, respectively. We first split the error of the quantization and the channel using the triangular inequality on every element of the gradient as follows

$$|g^n - \hat{g}^n|^2 \leq |g^n - \tilde{g}^n|^2 + |\tilde{g}^n - \hat{g}^n|^2. \quad (39)$$

We obtain upper bounds for each error term separately in the sequel. The expected value of the first term equals the variance of the quantization error, which is given by

$$\mathbb{E}[|g^n - \tilde{g}^n|^2] \leq \frac{1}{12K} \left(\frac{2\Delta_g}{q} \right)^2 = \frac{\Delta_g^2}{3Kq^2}. \quad (40)$$

Here, we obtained the variance under the assumption of a uniform distribution of the gradient elements. Then, for the second term, we follow the same procedure as the one used in [24, Theorem 1]. For the received signal at ES in Eq. (19), we can write

$$\begin{aligned} \hat{g}^n &= \frac{1}{K} \mathcal{D}_q \left(\sum_{k=1}^K \mathcal{E}_q(\tilde{g}_k^n) + \tilde{z}^n \right), \\ &= \tilde{g}^n + \frac{1}{K} \left(\Re(\mathcal{E}(\tilde{z}^n)) + 2^b \Im(\tilde{z}^n) \right). \end{aligned} \quad (41)$$

Then, we can write the MSE as follows

$$\mathbb{E}[|\tilde{g}^n - \hat{g}^n|_2^2] = \frac{1}{K^2} \mathbb{E}[|\Re(\tilde{z}^n)|_2^2] + \frac{2^{2b}}{K^2} \mathbb{E}[|\Im(\tilde{z}^n)|_2^2],$$

where the equality is due to that $\Re(\tilde{z}^n)$ and $\Im(\tilde{z}^n)$ are independent random variables. Furthermore, since the noise \tilde{z}^n is a circular AWGN, the variance of the noise is the

same for both real and imaginary parts. Thereafter, we define $e_r := |\Re(\tilde{z}^n)|_2^2 = |\Im(\tilde{z}^n)|_2^2$, which leads to

$$\mathbb{E}[|\tilde{g}^n - \hat{g}^n|_2^2] = \frac{(1+q)}{K^2} \mathbb{E}[e_r]. \quad (42)$$

Hence, we only require computing the term e_r . The noise \tilde{z}^n has Normal distribution $\mathcal{CN}(0, \sigma_z^2/\sqrt{N_r})$, so we can compute the expected value for e_r conditioned on $\Re(\tilde{z}^n)$ or $\Im(\tilde{z}^n)$ being between certain decision boundaries. Let P_ℓ be the probability that error becomes ℓ , i.e., $P_\ell := \Pr(e_r = \ell)$, then we have from [37, Section 6.1.4],

$$P_\ell = 2 \left(1 - \frac{\ell}{2^b}\right) \left(Q\left(\frac{(2\ell-1)\sqrt{N_r}}{\sigma_z}\right) - Q\left(\frac{(2\ell+1)\sqrt{N_r}}{\sigma_z}\right)\right).$$

Then, the expected value of the error is computed as

$$\begin{aligned} \mathbb{E}[e_r] &= \sum_{\ell=1}^{2^b-1} \ell^2 \times P_\ell, \\ &= 2 \sum_{\ell=1}^{2^b-1} \left(2\ell-1 \frac{3\ell-3\ell^2-1}{2^b}\right) Q\left(\frac{(2\ell-1)\sqrt{N_r}}{\sigma_z}\right). \end{aligned}$$

Next, we use the expression in Eqs. (42) and (40) to obtain an upper bound on the gradient average as follows.

$$\mathbb{E}[\|\mathbf{g} - \hat{\mathbf{g}}\|^2] \leq \frac{N(1+q)e_r}{K^2} + \frac{N\Delta_z^2}{3Kq^2}. \quad (43)$$

Finally, we conclude the proof.

C. Proof of Theorem 1

We define the error as $e^n := s^n - \hat{s}^n$, then use Eq. (8) to expand the error as follows

$$e^n = e_{\text{sig}}^n + e_{\text{int}}^n + e_{\text{noise}}^n, \quad (44)$$

where the terms are defined as

$$e_{\text{sig}}^n := \sum_{k=1}^K \left(\frac{\|\mathbf{h}_k^n\|^2}{\sigma_h^2 N_r} - 1 \right) s_k^n, \quad (45a)$$

$$e_{\text{int}}^n := \sum_{k,k',k \neq k'}^K \frac{\langle \mathbf{h}_k^n, \mathbf{h}_{k'}^n \rangle}{N_r \sigma_h^2} s_{k'}^n, \quad (45b)$$

$$e_{\text{noise}}^n := \sum_{k=1}^K \frac{\langle \mathbf{h}_k^n, \mathbf{z}_n \rangle}{\sigma_h^2 N_r}. \quad (45c)$$

Hence, the terms e_{sig}^n , e_{int}^n and e_{noise}^n are random variables with the following first and second order moments:

$$\mathbb{E}[e_{\text{sig}}^n] = 0, \quad \mathbb{E}[|e_{\text{sig}}^n|^2] = \alpha_1^n / N_r, \quad (46a)$$

$$\mathbb{E}[e_{\text{int}}^n] = 0, \quad \mathbb{E}[|e_{\text{int}}^n|^2] = \frac{(K-1)\alpha_2^n}{N_r}, \quad (46b)$$

$$\mathbb{E}[e_{\text{noise}}^n] = 0, \quad \mathbb{E}[|e_{\text{noise}}^n|^2] = K \frac{\sigma_z^2}{\sigma_h^2 N_r}, \quad (46c)$$

where $\alpha_1^n := 2 \sum_{k=1}^K |s_k^n|^2$, $\alpha_2^n := \sum_{k,k',k \neq k'}^K |s_k^n s_{k'}^n|$, and the expectations are over noise and channel coefficients distributions. In the following, we show how fast the tails of these random variables deviate from their expected values. To this end, we bring some relevant definitions and properties with Bernstein's inequality for obtaining upper bounds on their concentration.

Definition 1. For a random variable X with $\mathbb{E}[X] = 0$, we define

$$\lambda(X) := \inf\{t > 0 : \mathbb{E}[\exp(|X|/t)] \leq 2\}. \quad (47)$$

X is called a sub-exponential random variable with parameter λ , if $\lambda(X) < \infty$.

Lemma 1. ([38, Theorem 2.8.1]) Let X_1, \dots, X_n be independent random variables such that $\mathbb{E}[X_i] = 0$ and sub-exponential random variables with parameter λ . Then for any $t > 0$, we have

$$\mathbb{P}\left[\left|\frac{1}{n} \sum_{i=1}^n X_i\right| > t\right] \leq 2 \exp\left(-\frac{n}{2} \min\left(\frac{t^2}{\lambda^2}, \frac{t}{\lambda}\right)\right). \quad (48)$$

In the sequel, we show that each error term in Eq. (45), vanishes for a large enough number of antennas N_r using Lemma 1. For the first error term, e_{sig}^n , we have the following Lemma.

Lemma 2. Let $\epsilon_1 > 0$ and $\delta_1 > 0$ be positive scalars. Then, the absolute value of the signal error in Eq. (45a), $|e_{\text{sig}}^n|$, is upper bounded by the scalar ϵ_1 with probability at least $1 - \delta_1$, if

$$N_r \geq \frac{4\gamma_n^2}{\epsilon_1^2} \ln\left(\frac{2K}{\delta_1}\right), \quad (49)$$

where $\gamma_n = \sum_k^K |s_k^n|$.

Proof. See Appendix D. \square

Lemma 3. Let $\epsilon_2 > 0$ and $\delta_2 > 0$ be positive scalars. Then, the absolute value of the interference error term in Eq. (45b), $|e_{\text{int}}^n|$, is upper bounded by the scalar ϵ_2 with probability at least $1 - \delta_2$, if

$$N_r \geq \frac{8(K-1)^2 \gamma_n^2}{\epsilon_2^2} \ln\left(\frac{2(K-1)}{\delta_2}\right), \quad (50)$$

where $\gamma_n = \sum_k^K |s_k^n|$.

Proof. See Appendix E. \square

Lemma 4. Let $\epsilon_3 > 0$ and $\delta_3 > 0$ be positive scalars. Then, the absolute value of the noise error in Eq. (45c), $|e_{\text{noise}}^n|$, is upper bounded by the scalar ϵ_3 with probability at least $1 - \delta_3$, if

$$N_r \geq \frac{8\sigma_z^2 K^2}{\sigma_h^2 \epsilon_3^2} \ln\left(\frac{2(K-1)}{\delta_3}\right), \quad (51)$$

where $\gamma_n = \sum_k^K |s_k^n|$.

Proof. See Appendix F. \square

From Lemmas 2, 3, and 4, we can bound the absolute value of the defined error in Eq. (44), as follows

$$\begin{aligned} |e^n| &= |e_{\text{sig}}^n + e_{\text{int}}^n + e_{\text{noise}}^n| \leq |e_{\text{sig}}^n| + |e_{\text{int}}^n| + |e_{\text{noise}}^n|, \\ &\leq \epsilon_1 + \epsilon_2 + \epsilon_3 \leq \epsilon. \end{aligned} \quad (52)$$

Due to the union bound, the events of Lemmas 2, 3, and 4 hold simultaneously with probability no less than $1 - (\delta_1 + \delta_2 + \delta_3)$ or $1 - \delta$, where $\delta \geq \delta_1 + \delta_2 + \delta_3$ [39], [40]. Thus, this proves Eq. (25).

To satisfy all the constraints in Lemmas 2, 3, and 4, the number of antennas needs to be greater than all the inequalities, i.e.,

$$N_r \geq \max \left\{ \frac{4\gamma_n^2}{\epsilon_1^2} \ln \left(\frac{2K}{\delta_1} \right), \frac{8(K-1)^2\gamma_n^2}{\epsilon_2^2} \ln \left(\frac{2(K-1)}{\delta_2} \right), \frac{8\sigma_z^2 K^2}{\sigma_h^2 \epsilon_3^2} \ln \left(\frac{2(K-1)}{\delta_3} \right) \right\}. \quad (53)$$

For further simplifications, we can set $\delta_1 = \delta/3$, $\delta_2 = (1-1/K)\delta/3$, and $\delta_3 = (1-1/K)\delta/3$, which leads to

$$\delta_1 + \delta_2 + \delta_3 \leq \frac{\delta}{3} \left(1 + 1 + 1 - \frac{2}{K} \right) \leq \delta. \quad (54)$$

Moreover, we obtain the following lower bound for N_r :

$$N_r \geq \max \left\{ \frac{4\gamma_n^2}{\epsilon_1^2}, \frac{8(K-1)^2\gamma_n^2}{\epsilon_2^2}, \frac{8\sigma_z^2 K^2}{\sigma_h^2 \epsilon_3^2} \right\} \ln \left(\frac{6K}{\delta} \right).$$

Next, let us rewrite ϵ_1 , ϵ_2 , and ϵ_3 as follows.

$$\epsilon_1 = \frac{\sigma_h}{\sigma_z K} \epsilon'', \quad (55a)$$

$$\epsilon_2 = \frac{\sigma_h(K-1)}{\sqrt{2}\sigma_z K} \epsilon'', \quad (55b)$$

$$\epsilon_3 = \frac{1}{\sqrt{2}\gamma_n} \epsilon'', \quad (55c)$$

for some positive value $\epsilon'' > 0$. Hence, we have that $\epsilon_1 + \epsilon_2 + \epsilon_3 < \epsilon'' \left(\frac{\sigma_h}{\sqrt{2}\sigma_z} + \frac{1}{\sqrt{2}\gamma_n} \right)$. Then, by setting $\epsilon = \epsilon'' c_n / \sqrt{2}$, where $c_n = \sigma_h / \sigma_z + 1/\gamma_n$, we obtain the following expression for N_r :

$$N_r \geq \frac{8\gamma_n^2 \sigma_z^2 K^2}{\sigma_h^2 \epsilon^2 c_n^2} \ln \left(\frac{6K}{\delta} \right).$$

This proves Eq. (26). Then, for the expected value in Eq. (25), from [41][Theorem 1.6.2], we know that the expected values of the bounded random variable, e^n , can also be bounded as follows:

$$\mathbb{E}[e^n] \leq \frac{4K\gamma_n}{\sqrt{N_r} c_n} (\sqrt{\pi} + \ln(6K)). \quad (56)$$

Thus, we conclude the proof for Theorem 1.

D. Proof of Lemma 2

We first define the variable Y_ℓ for $\ell \in [N_r]$ as follows:

$$Y_\ell^k := \frac{1}{\sigma_h^2} (h_{k,\ell}^n)^2, \quad \forall k \in [K], \quad n \in [N], \quad (57)$$

which yields $\sum_{\ell=1}^{N_r} Y_\ell^k / N_r = \|\mathbf{h}_k^n\|^2 / N_r \sigma_h^2$. Due to the Normal distribution assumption on $h_{k,\ell}^n$ from Section II-B, Y_ℓ^k is sub-exponential with parameters (2, 4). Consequently, since the variables Y_ℓ^k are independent for $(\ell, k) \in [N_r] \times [K]$, the average $\sum_{\ell=1}^{N_r} Y_\ell^k / N_r$ has Chi-squared distribution with N_r degrees of freedom. To bound this variable, we use Lemma 5.

Lemma 5. [42, Lemma 1] *Let (Y_1, \dots, Y_n) be iid Normal random variables. We set $Y = \sum_{i=1}^n Y_i^2 - n$. Then, the following inequalities hold for any positive t :*

$$\mathbb{P}(Y \geq 2\sqrt{nt} + 2t) \leq \exp(-t), \quad (58a)$$

$$\mathbb{P}(Y \leq -2\sqrt{nt}) \leq \exp(-t). \quad (58b)$$

By applying Lemma 5, the variable $\sum_{\ell=1}^{N_r} Y_\ell^k / N_r$ is bounded below as

$$\left| \frac{\sum_{\ell=1}^{N_r} Y_\ell^k}{N_r} - 1 \right| \geq c_1, \quad k \in [K], \quad (59)$$

with probability at most $\exp(-N_r c_1^2/4) + \exp(-N_r c_1^2/2) \leq 2 \exp(-N_r c_1^2/4)$ for each term. Invoking the union bound, the probability that at least one of the events in Eq. (59) occurs is at most

$$\sum_{k=1}^K \Pr \left(\left| \frac{\sum_{\ell=1}^{N_r} Y_\ell^k}{N_r} - 1 \right| \geq c_1 \right) \leq K \times 2 \exp(-N_r c_1^2/4).$$

Hence, all the terms for the variable $\sum_{\ell=1}^{N_r} Y_\ell^k / N_r$ are bounded above as

$$\left| \frac{\sum_{\ell=1}^{N_r} Y_\ell^k}{N_r} - 1 \right| \leq c_1, \quad k \in [K], \quad (60)$$

with probability at least $1 - 2K \exp(-N_r c_1^2/4)$. Accordingly, for the error e_{sig}^n , we can use Eqs. (45) as follows:

$$\begin{aligned} |s^n - s_{\text{sig}}^n| &= \left| \sum_{k=1}^K \left(\frac{\sum_{\ell=1}^{N_r} Y_\ell^k}{N_r} - 1 \right) s_k^n \right| \\ &\leq \sum_{k=1}^K \left| \frac{\sum_{\ell=1}^{N_r} Y_\ell^k}{N_r} - 1 \right| |s_k^n| \leq c_1 \sum_{k=1}^K |s_k^n| \\ &= c_1 \gamma_n, \end{aligned} \quad (61)$$

where the first inequality is the triangle inequality, and the second inequality uses the upper bound in Eq. (60). Also, γ_n is defined as

$$\gamma_n := \sum_{k=1}^K |s_k^n|. \quad (62)$$

To bound e_{sig}^n from above by ϵ_1 , we have to bound c_1 to be $c_1 \gamma_n \leq \epsilon_1$, or, equivalently, $c_1 \leq \epsilon_1 / \gamma_n$. As a result, the error term is upper bounded by ϵ_1 , i.e., $e_{\text{sig}}^n \leq \epsilon_1$, with probability at least $1 - \delta_1$ as long as the following inequality on δ_1 is satisfied:

$$K \times 2 \exp(-N_r c_1^2/4) \leq \delta_1. \quad (63)$$

Hence, we rearrange the expression in Eq. (63) to have N_r on the left side hand of the inequality, i.e.,

$$N_r \geq \frac{4\gamma_n^2}{\epsilon_1^2} \ln \left(\frac{2K}{\delta_1} \right), \quad (64)$$

where the last inequality is fulfilled due to c_1 being upper bounded by ϵ_1 / γ_n . Therefore, the proof is concluded.

E. Proof of Lemma 3

Let us define the variable X_ℓ for $\ell \in [N_r]$ as follows,

$$X_\ell^{(k,k')} := \frac{1}{\sigma_h^2} h_{k,\ell}^n h_{k',\ell}^n, \quad \text{for } k, k' \in [K], \quad n \in [N]. \quad (65)$$

Consequently, we have

$$\frac{1}{N_r} \sum_{\ell=1}^{N_r} X_\ell^{(k,k')} = \frac{1}{N_r \sigma_h^2} \langle \mathbf{h}_k^n, \mathbf{h}_{k'}^n \rangle. \quad (66)$$

Considering that $h_{k,\ell}^n/\sigma_h$ and $h_{k',\ell}^n/\sigma_h$ are Normal random variables, the product of them in Eq. (65) makes $X_\ell^{(k,k')}$ sub-exponential with $\lambda = 2$ [38, Lemma 2.7.7]. Therefore, the direct results of applying Lemma 1 to the term $\frac{1}{N_r\sigma_h^2}\langle \mathbf{h}_k^n, \mathbf{h}_{k'}^n \rangle$, gives us the following upper bound

$$\left| \frac{1}{N_r} \sum_{\ell=1}^{N_r} X_\ell^{(k,k')} \right| \leq c_2, \quad (67)$$

with the probability at least $1 - 2\exp(-N_r c_2^2/8)$. Hence, to make sure that $|s_{\text{int}}^n|$ is bounded by ϵ_2 with probability at least $1 - \delta_2$, we have

$$\begin{aligned} |s_{\text{int}}^n| &= \left| \sum_{k,k',k \neq k'}^K \frac{\langle \mathbf{h}_k^n, \mathbf{h}_{k'}^n \rangle}{N_r \sigma_h^2} s_{k'}^n \right| \leq \sum_{k,k',k \neq k'}^K \left| \frac{1}{N_r} X_\ell^{(k,k')} \right| |s_{k'}^n|, \\ &\leq (K-1)c_2 \sum_k^K |s_k^n|. \end{aligned} \quad (68)$$

Then, let us define $\gamma_n := \sum_k^K |s_k^n|$, such that

$$(K-1)c_2\gamma_n \leq \epsilon_2 \Rightarrow c_2 \leq \frac{\epsilon_2}{(K-1)\gamma_n}. \quad (69)$$

Using the same arguments from Appendix D, the condition in Eq. (67) can be satisfied for all $k, k' \in [K]$ with probability at least

$$1 - (K-1) \times 2 \exp(-N_r c_2^2/8). \quad (70)$$

Then, the number of required antennas N_r needs to fulfill the inequality below:

$$\begin{aligned} (K-1) \times 2 \exp(-N_r c_2^2/8) &\leq \delta_2, \\ -N_r c_2^2/8 &\leq \ln\left(\frac{\delta_2}{2(K-1)}\right), \\ N_r &\geq \frac{8}{c_2^2} \ln\left(\frac{2(K-1)}{\delta_2}\right). \end{aligned} \quad (71)$$

Afterward, by substituting Eq. (69) into Eq. (71), we obtain

$$N_r \geq \frac{8(K-1)^2 \gamma_n^2}{c_2^2} \ln\left(\frac{2(K-1)}{\delta_2}\right). \quad (72)$$

Using Eq. (72), we conclude the proof.

F. Proof of Lemma 4

Let W_ℓ be defined as

$$W_\ell := \frac{h_{k,\ell}^n z_\ell^n}{\sigma_h \sigma_h}, \quad \forall k \in [K], n \in [N], \quad (73)$$

where $\ell \in [N_r]$. Here, $h_{k,\ell}^n/\sigma_h$ and z_ℓ^n/σ_h are two sub-Gaussian random variables with parameters 1 and σ_z^2/σ_h^2 , respectively. Thus, W_ℓ is a sub-exponential random variable with parameter $\lambda = 2 \times 1 \times \sigma_z/\sigma_h$ [43]. Similar to Eq. (67) in Appendix E, we apply Lemma 1 to bound the summation $\sum_{\ell=1}^{N_r} W_\ell$ as follows

$$\left| \frac{1}{N_r} \sum_{\ell=1}^{N_r} W_\ell \right| = \left| \frac{1}{N_r \sigma_h^2} \langle \mathbf{h}_k^n, \mathbf{z}_n \rangle \right| \leq c_3, \quad (74)$$

with probability no less than $1 - 2\exp(-N_r \sigma_h^2 c_3^2/8\sigma_z^2)$. Therefore, e_{noise}^n is bounded from above as follows

$$|e_{\text{noise}}^n| = \left| \sum_{k=1}^K \frac{\langle \mathbf{h}_k^n, \mathbf{z}_n \rangle}{\sigma_h^2 N_r} \right| \leq K c_3 \leq \epsilon_3. \quad (75)$$

Hence, $c_3 \leq \epsilon_3/K$.

Then, by using the union bound similar to Appendix D, for all k items of e_{noise}^n , we have $2K \exp(-N_r \sigma_h^2 c_3^2/8\sigma_z^2)$ to be lower than δ_3 , which leads to

$$N_r \geq \frac{8\sigma_z^2}{\sigma_h^2 c_3^2} \ln\left(\frac{2(K-1)}{\delta_3}\right). \quad (76)$$

By setting $c_3 = \epsilon_3/K$, we obtain

$$N_r \geq \frac{8\sigma_z^2 K^2}{\sigma_h^2 \epsilon_3^2} \ln\left(\frac{2(K-1)}{\delta_3}\right). \quad (77)$$

Thus, we can conclude the proof.

G. Proof of Proposition 3

To obtain an upper bound on the MSE of \mathbf{g} , we use the triangular inequality to split the channel and quantization errors as follows:

$$\|\mathbf{g} - \hat{\mathbf{g}}\|^2 \leq \|\mathbf{g} - \tilde{\mathbf{g}}\|^2 + \|\tilde{\mathbf{g}} - \hat{\mathbf{g}}\|^2, \quad (78)$$

where the first error term is due to the quantization error, and the second term represents the channel errors. Considering the fact that the elements of gradient \mathbf{g} are bounded by value Δ_q , the expected value of the first term is bounded as

$$\mathbb{E}[\|\mathbf{g} - \tilde{\mathbf{g}}\|^2] \leq \frac{N\Delta_q^2}{3Kq^2}. \quad (79)$$

To upper bound the absolute error of the gradient $\tilde{\mathbf{g}}$ and $\hat{\mathbf{g}}$, we first need to obtain an upper bound on the error of every element. Due to the channel fading and noise, the transmitted gradient over sub-channel n -th, i.e., \tilde{g}_k^n in Eq. (38) is contaminated with error. Hence, the estimated gradient can be written as

$$\begin{aligned} \hat{g}^n &= \frac{1}{K} \mathcal{D}_q\left(\sum_{k=1}^K \mathcal{E}_q(\tilde{g}_k^n) + e_{ch}\right), \\ &= \frac{1}{K} \Re\left(\sum_{k=1}^K \mathcal{E}_q(\tilde{g}_k^n) + e_{ch}\right) \\ &\quad + \frac{2^b}{K} \left(\Im\left(\frac{1}{K} \sum_{k=1}^K \mathcal{E}_q(\tilde{g}_k^n) + e_{ch}\right) + \frac{2^b+1}{2} \right) + \frac{2^b-1}{2}, \\ &= \tilde{g}^n + \frac{1}{K} \Re(e_{ch}) + \frac{2^b}{K} \cdot \Im(e_{ch}). \end{aligned} \quad (80)$$

As a result, for the error $e_g := |\hat{g}^n - \tilde{g}^n|$, we have

$$\begin{aligned} |\hat{g}^n - \tilde{g}^n| &= \frac{1}{K} |\Re(e_{ch}) + 2^b \cdot \Im(e_{ch})|, \\ &\leq \frac{1}{K} |\Re(e_{ch})| + \frac{2^b}{K} |\Im(e_{ch})|. \end{aligned} \quad (81)$$

Then, for $N_r \geq \frac{8\sigma_z^2 K^2}{\sigma_h^2 \epsilon^2} \ln\left(\frac{6K}{\delta}\right)$ Theorem 1, we can bound the error as follows

$$|\hat{g}^n - \tilde{g}^n| \leq \frac{1}{K} (\epsilon + 2^b \epsilon) = \frac{(2^b+1)}{K} \epsilon. \quad (82)$$

Afterward, we use Eq. (82) to obtain an upper bound on the whole gradient as

$$\|\tilde{\mathbf{g}} - \hat{\mathbf{g}}\|^2 \leq N(2^{2b} + 1 + 2^{b+1}) \frac{\epsilon^2}{K^2} \leq 2Nq \frac{\epsilon^2}{K^2}. \quad (83)$$

By defining $\epsilon_{\text{fad}}^2 := 2Nq\epsilon^2/K^2$, we can complete the proof for Eq. (27). Next, to obtain an upper bound for the expected value, we use the same argument in Eq. (82) from Appendix C for bounded variables in $|\hat{g}^n - \tilde{g}^n|$, which leads to the following:

$$\mathbb{E}[|\hat{g}^n - g^n|] \leq 4 \frac{(\sqrt{q} + 1)\gamma_n}{\sqrt{N_r}c_n} (\sqrt{\pi} + \ln(6K)). \quad (84)$$

Hence, for the norm of $\mathbf{g} - \hat{\mathbf{g}}$, we have

$$\begin{aligned} \mathbb{E}[\|\mathbf{g} - \hat{\mathbf{g}}\|^2] &\leq 16 \frac{qN \max_n \gamma_n^2}{N_r \min_n c_n^2} (\pi + 2 \ln(6K))^2, \\ &\leq 16 \frac{qN \gamma_{\max}^2}{N_r c_{\min}^2} (\pi + 2 \ln(6K))^2. \end{aligned} \quad (85)$$

Finally, by taking expectation over both sides of Eq. (78) and substituting the upper bound in Eq. (85), we obtain

$$\mathbb{E}[\|\mathbf{g} - \hat{\mathbf{g}}\|^2] \leq \sigma_q^2 + 16 \frac{qN \gamma_{\max}^2}{N_r c_{\min}^2} (\pi + 2 \ln(6K))^2. \quad (86)$$

This concludes the proof.

H. Proof of Proposition 4

The proof herein follows the same procedure used in [18], [20], [21]. By using Assumption 2, we can write the following upper bound for the loss functions of two consecutive communication rounds:

$$\mathcal{L}(\mathbf{g}(m+1)) - \mathcal{L}(\mathbf{g}(m)) \leq -\eta \langle \mathbf{g}(m), \hat{\mathbf{g}}(m) \rangle + \frac{\eta^2 L}{2} \|\hat{\mathbf{g}}(m)\|^2.$$

Here, we have $\mathbf{w}(m+1) = \mathbf{w}(m) - \eta \hat{\mathbf{g}}(m)$. Taking the expectation from both sides of an inequality, we get the following

$$\begin{aligned} \mathbb{E}[\mathcal{L}(\mathbf{g}(m+1)) - \mathcal{L}(\mathbf{g}(m))] &\leq -\eta \langle \mathbf{g}(m), \mathbb{E}[\hat{\mathbf{g}}] \rangle \\ &\quad + \frac{\eta^2 L}{2} \mathbb{E}[\|\hat{\mathbf{g}}(m)\|^2], \\ &= -\eta \|\mathbf{g}(m)\|^2 + \frac{\eta^2 L}{2} \mathbb{E}[\|\hat{\mathbf{g}}(m)\|^2], \\ &\leq -\eta \|\mathbf{g}(m)\|^2 + \frac{\eta^2 L}{2} ((\sigma_{\text{ch}}^2 + \sigma_q^2) + \bar{\theta}), \end{aligned}$$

where the first equality is due to Assumption 4, and the inequality comes from the upper bounds on the variance of the quantization error and gradient variance in Assumptions 3 and 4, respectively. Also, to obtain the inequality $\mathbb{E}[\|\mathbf{g} - \tilde{\mathbf{g}}\|^2] \leq \frac{N\Delta_q^2}{Kq^2}$, we used Popoviciu's inequality [44] for the variance of bounded variables, $|g_k^n| \leq \Delta_q$ for $k \in [K]$. Then, by performing a telescoping sum over the communication rounds

and subtracting the $\mathcal{L}(\mathbf{g}^*)$ from both sides of the inequality, we get the following.

$$\begin{aligned} \mathcal{L}(\mathbf{g}^{(1)}) - \mathcal{L}(\mathbf{g}^*) &\geq \mathcal{L}(\mathbf{g}(1)) - \mathbb{E}[\mathcal{L}(\mathbf{g}(T))], \\ &= \mathbb{E} \left[\sum_{m=1}^T \mathcal{L}(\mathbf{w}(m)) - \mathcal{L}(\mathbf{w}(m-1)) \right], \\ &\geq \sum_{m=1}^T \mathbb{E} \left[\mathcal{L}(\mathbf{w}(m)) - \mathcal{L}(\mathbf{w}(m-1)) \right] \\ &\geq (-\eta + \frac{\eta^2 L}{2}) \mathbb{E} \left[\sum_{m=1}^T \|\mathbf{g}(m)\|^2 \right] \\ &\quad + \frac{\eta^2 L T}{2} (\sigma_{\text{ch}}^2 + \sigma_q^2 + \bar{\theta}). \end{aligned} \quad (87)$$

Finally, rearranging the last inequality concludes the proof.

I. Latency Analysis

To derive the latency for the fading channel, the transmission rate-distortion function of the communication scheme is needed. In particular, to calculate the rate-distortion function for a fading channel with bandwidth B , taking into account an MSE distortion measure, the following formula from [36] is used:

$$\mathcal{R}(\sigma_d^2) = \max[B \ln \left(\frac{\sigma_s^2}{\sigma_d^2} \right), 0], \quad (88)$$

where σ_s^2 is the signal power and σ_d^2 is the distortion. In our MIMO fading channel scenario in (8), the distortion σ_d^2 after beamforming and averaging is expressed as:

$$\sigma_{\text{d-Analog}}^2 = \frac{\sigma_z^2}{N_r K \sigma_h^2} + \frac{(K-1)\sigma_{\text{int}}^2}{3N_r}, \quad (89)$$

$$\sigma_{\text{s-Analog}}^2 = \sum_{k=1}^K |s_k^n|^2 / K, \quad (90)$$

where $\sigma_{\text{int}}^2 = \sum_{k,k',k \neq k'}^K \mathbb{E}[|s_k^n s_{k'}^n|]$. Hence, to quantify the latency for analog OAC, the equation is formulated as follows:

$$T_{\text{ana}} := \frac{T_s N}{\mathcal{R}(\sigma_{\text{d-Analog}}^2)} = \frac{T_s}{B} \frac{N}{\ln(\sigma_{\text{s-Analog}}^2 / \sigma_{\text{d-Analog}}^2)}, \quad (91)$$

where T_s represents the duration of an OFDM symbol, and N indicates the model size, i.e., the number of model parameters.

For ChannelCompFed to adhere to a similar rate-distortion function, it experiences distinct distortions, described by:

$$\sigma_{\text{d-CompFed}}^2 = \frac{\Delta_q^2}{q^2 K} + \frac{(1+q)\tilde{e}_r^2}{K^2}, \quad (92a)$$

$$\sigma_{\text{s-CompFed}}^2 = \sum_{k=1}^K |s_k^n|^2 / K \left| \frac{2q^2}{q+1} \right|, \quad (92b)$$

where $\frac{\Delta_q^2}{q^2}$ represents the quantization error and $\frac{2q^2}{q+1}$ arises from the fact that QAM modulation consumes $\frac{2q^2}{q+1}$ less power than its analog counterpart. The error term \tilde{e}_r is the same as the error term defined in (23) while the variance σ_z needs to be replaced by $\sigma_{\text{d-Analog}}^2$. Consequently, the latency for ChannelCompFed is given by:

$$T_{\text{CompFed}} := \frac{T_s N}{\mathcal{R}(\sigma_{\text{d-CompFed}}^2)} = \frac{T_s}{B} \frac{N}{\ln(\sigma_{\text{s-CompFed}}^2 / \sigma_{\text{d-CompFed}}^2)},$$

Thus, the latency reduction ratio of ChannelCompFed over its analog counterpart is defined as:

$$\gamma := \frac{T_{\text{CompFed}}}{T_{\text{ana}}} = \frac{\ln(\sigma_{\text{s-Analog}}^2/\sigma_{\text{d-Analog}}^2)}{\ln(\sigma_{\text{s-CompFed}}^2/\sigma_{\text{d-CompFed}}^2)}. \quad (93)$$

As q increases in (92a) and (92b), the latency reduction ratio γ approaches one, indicating asymptotic performance equivalence. However, ChannelCompFed can facilitate low latency communication at low quantization levels, although with higher quantization errors.

REFERENCES

- [1] T. Li, A. K. Sahu, A. Talwalkar, and V. Smith, "Federated learning: Challenges, methods, and future directions," *IEEE Sig. Process. Mag.*, vol. 37, no. 3, pp. 50–60, 2020.
- [2] J. Konečný, H. B. McMahan, F. X. Yu, P. Richtárik, A. T. Suresh, and D. Bacon, "Federated learning: Strategies for improving communication efficiency," *arXiv preprint arXiv:1610.05492*, 2016.
- [3] S. M. Azimi-Abarghouyi and V. Fodor, "Multi-server over-the-air federated learning," *arXiv preprint arXiv:2211.16162*, 2022.
- [4] B. McMahan, E. Moore, D. Ramage, S. Hampson, and B. A. y Arcas, "Communication-efficient learning of deep networks from decentralized data," in *Artificial intelligence and statistics*. PMLR, 2017, pp. 1273–1282.
- [5] A. Tak and S. Cherkaoui, "Federated edge learning: design issues and challenges," *IEEE Network*, vol. 35, no. 2, pp. 252–258, 2020.
- [6] G. Zhu, Y. Wang, and K. Huang, "Broadband analog aggregation for low-latency federated edge learning," *IEEE Trans. Wireless Commun.*, vol. 19, no. 1, pp. 491–506, 2019.
- [7] M. Goldenbaum, H. Boche, and S. Stańczak, "Nomographic functions: Efficient computation in clustered Gaussian sensor networks," *IEEE Trans. Wireless Commun.*, vol. 14, no. 4, pp. 2093–2105, 2014.
- [8] H. Hellström, J. M. B. da Silva Jr, M. M. Amiri, M. Chen, V. Fodor, H. V. Poor, C. Fischione *et al.*, "Wireless for machine learning: A survey," *Foundations and Trends® in Sig. Process.*, vol. 15, no. 4, pp. 290–399, 2022.
- [9] K. Yang, T. Jiang, Y. Shi, and Z. Ding, "Federated learning via over-the-air computation," *IEEE Trans. Wireless Commun.*, vol. 19, no. 3, pp. 2022–2035, 2020.
- [10] Y.-S. Jeon, M. M. Amiri, J. Li, and H. V. Poor, "A compressive sensing approach for federated learning over massive MIMO communication systems," *IEEE Trans. Wireless Commun.*, vol. 20, no. 3, pp. 1990–2004, 2020.
- [11] M. M. Amiri and D. Gündüz, "Federated learning over wireless fading channels," *IEEE Trans. Wireless Commun.*, vol. 19, no. 5, pp. 3546–3557, 2020.
- [12] Y. Shao, D. Gündüz, and S. C. Liew, "Federated edge learning with misaligned over-the-air computation," *IEEE Trans. Wireless Commun.*, vol. 21, no. 6, pp. 3951–3964, November 2021.
- [13] S. Razavikia, J. A. Peris, J. M. B. Da Silva, and C. Fischione, "Blind asynchronous over-the-air federated edge learning," in *IEEE Globecom Workshops*, 2022, pp. 1834–1839.
- [14] H. Hellström, S. Razavikia, V. Fodor, and C. Fischione, "Optimal receive filter design for misaligned over-the-air computation," *arXiv preprint arXiv:2309.16033*, 2023.
- [15] B. Tegin and T. M. Duman, "Blind federated learning at the wireless edge with low-resolution ADC and DAC," *IEEE Trans. Wireless Commun.*, vol. 20, no. 12, pp. 7786–7798, 2021.
- [16] M. M. Amiri, T. M. Duman, D. Gündüz, S. R. Kulkarni, and H. V. Poor, "Blind federated edge learning," *IEEE Trans. Wireless Commun.*, vol. 20, no. 8, pp. 5129–5143, 2021.
- [17] A. Şahin, B. Everette, and S. S. M. Hoque, "Distributed learning over a wireless network with FSK-based majority vote," in *CommNet*. IEEE, 2021, pp. 1–9.
- [18] G. Zhu, Y. Du, D. Gündüz, and K. Huang, "One-bit over-the-air aggregation for communication-efficient federated edge learning: Design and convergence analysis," *IEEE Trans. Wireless Commun.*, vol. 20, no. 3, pp. 2120–2135, 2020.
- [19] X. Zhao, L. You, R. Cao, Y. Shao, and L. Fu, "Broadband digital over-the-air computation for asynchronous federated edge learning," in *ICC*. IEEE, 2022, pp. 5359–5364.
- [20] J. Bernstein, Y.-X. Wang, K. Azizzadenesheli, and A. Anandkumar, "signSGD: Compressed optimisation for non-convex problems," in *Int. Conf. Mach. Learn.* PMLR, 2018, pp. 560–569.
- [21] A. Şahin, "Over-the-air computation based on balanced number systems for federated edge learning," *IEEE Trans. on Wireless Commun.*, 2023.
- [22] S. Razavikia, J. M. B. Da Silva, and C. Fischione, "ChannelComp: A general method for computation by communications," *IEEE Trans. on Commun.*, 2023.
- [23] S. Razavikia, J. M. B. d. Silva Jr, and C. Fischione, "Computing functions over-the-air using digital modulations," in *IEEE ICC*, 2023, pp. 5780–5786.
- [24] —, "SumComp coding: Digital over-the-air computation via the ring of integers," *arXiv preprint arXiv:2310.20504*, 2023.
- [25] M. I. Jordan, J. D. Lee, and Y. Yang, "Communication-efficient distributed statistical inference," *Journal of the American Statistical Association*, 2018.
- [26] P. Yang, Y. Jiang, T. Wang, Y. Zhou, Y. Shi, and C. N. Jones, "Over-the-air federated learning via second-order optimization," *IEEE Trans. Wireless Commun.*, vol. 21, no. 12, pp. 10560–10575, 2022.
- [27] H. Hellstrom, V. Fodor, and C. Fischione, "Federated learning over-the-air by retransmissions," *IEEE Trans. Wireless Commun.*, vol. Early Access, 2023.
- [28] F. Rusek, D. Persson, B. K. Lau, E. G. Larsson, T. L. Marzetta, O. Edfors, and F. Tufvesson, "Scaling up MIMO: Opportunities and challenges with very large arrays," *IEEE Sig. Process. Mag.*, vol. 30, no. 1, pp. 40–60, 2012.
- [29] D. Astely, P. Von Butovitsch, S. Faxér, and E. Larsson, "Meeting 5g network requirements with massive mimo," *Ericsson Technology Review*, vol. 2022, no. 1, pp. 2–11, 2022.
- [30] L. Clavier, T. Pedersen, I. Larrad, M. Lauridsen, and M. Egan, "Experimental evidence for heavy tailed interference in the iot," *IEEE Communications Letters*, vol. 25, no. 3, pp. 692–695, 2020.
- [31] D. Middleton, "Statistical physical models of electromagnetic interference," *IEEE Transactions on Electromagnetic Compatibility*, vol. EMC-19, no. 3, pp. 106–127, 1977.
- [32] H. H. Yang, Z. Chen, T. Q. Quek, and H. V. Poor, "Revisiting analog over-the-air machine learning: The blessing and curse of interference," *IEEE Journal of Selected Topics in Signal Processing*, vol. 16, no. 3, pp. 406–419, 2021.
- [33] Y. LeCun, "The MNIST database of handwritten digits," <http://yann.lecun.com/exdb/mnist/>, 1998.
- [34] A. Krizhevsky, G. Hinton *et al.*, "Learning multiple layers of features from tiny images," 2009.
- [35] D. P. Kingma and J. Ba, "Adam: A method for stochastic optimization," *arXiv preprint arXiv:1412.6980*, 2014.
- [36] F. Hekland, P. A. Floor, and T. A. Ramstad, "Shannon-kotel-nikov mappings in joint source-channel coding," *IEEE Transactions on Communications*, vol. 57, no. 1, pp. 94–105, 2009.
- [37] A. Goldsmith, *Wireless communications*. Cambridge university press, 2005.
- [38] R. Vershynin, "High-dimensional probability," *University of California, Irvine*, 2020.
- [39] S. Razavikia, A. Amini, and S. Daei, "Reconstruction of binary shapes from blurred images via Hankel-structured low-rank matrix recovery," *IEEE Trans. on Image Processing*, vol. 29, pp. 2452–2462, 2020.
- [40] M. Bokaei, S. Razavikia, S. Rini, A. Amini, and H. Behrouzi, "Harmonic retrieval using weighted lifted-structure low-rank matrix completion," *Elsevier Signal Processing*, p. 109253, 2023.
- [41] J. A. Tropp *et al.*, "An introduction to matrix concentration inequalities," *Foundations and Trends® in Machine Learning*, vol. 8, no. 1-2, pp. 1–230, 2015.
- [42] B. Laurent and P. Massart, "Adaptive estimation of a quadratic functional by model selection," *The Annals of Statistics*, vol. 28, no. 5, pp. 1302–1338, 2000.
- [43] M. J. Wainwright, *High-dimensional statistics: A non-asymptotic viewpoint*. Cambridge university press, 2019, vol. 48.
- [44] R. Bhatia and C. Davis, "A better bound on the variance," *The american mathematical monthly*, vol. 107, no. 4, pp. 353–357, 2000.